Breakdown of the Landau-Fermi liquid in two dimensions due to umklapp scattering

C. Honerkamp,[1] M. Salmhofer,[2] N. Furukawa,[1,3] and T. M. Rice[1]
[1]*Theoretische Physik, ETH-Hönggerberg, CH-8093 Zürich, Switzerland*
[2]*Mathematik, ETH Zentrum, CH-8092 Zürich, Switzerland*
[3]*Department of Physics, Aoyama Gakuin University, Setagaya, Tokyo 157-8572, Japan**
(Received 23 December 1999; published 2 January 2001)

We study the renormalization-group (RG) flow of interactions in the two-dimensional t-t' Hubbard model near half-filling in an N-patch representation of the whole Fermi surface. Starting from weak to intermediate couplings the flows are to strong coupling, with different characters depending on the choice of parameters. In a large parameter region elastic umklapp scatterings drive an instability which on parts of the Fermi surface exhibits the key signatures of an insulating spin liquid (ISL), as proposed by Furukawa, Rice, and Salmhofer [Phys. Rev. Lett. **81**, 3195 (1998)] rather than a conventional symmetry-broken state. The ISL is characterized by both strong d-wave pairing and antiferromagnetic correlations; however, it is insulating due to the vanishing local charge compressibility and a spin liquid because of the spin gap arising from the pairing correlations. We find that the unusual RG flow, which we interpret in terms of an ISL, is a consequence of a Fermi surface close to the saddle points at the Brillouin-zone boundaries which provides an intrinsic and mutually reinforcing coupling between pairing and umklapp channels.

DOI: 10.1103/PhysRevB.63.035109 PACS number(s): 71.10.Hf, 71.27.+a, 74.72.−h

I. INTRODUCTION

The Landau theory is widely used to describe Fermi liquids even when the interactions are strong, but it cannot be justified *a priori*. The cuprate high-T_c superconductors show clear deviations from Landau theory in the normal state, and it has long been argued that the key to understanding these materials lies in the breakdown of Landau theory.[1] One possible cause is a symmetry-breaking instability such as magnetic order. But in experiments on underdoped cuprates,[2] the marked deviations from Landau theory, such as the onset of the spin gap and gaps in the angle-resolved photoemission spectra near the saddle points of the Fermi surface (FS), appear without an obvious symmetry breaking. This raises the question of whether a breakdown of Landau theory without symmetry breaking is possible. Actually one example is well known and understood, the insulating spin liquid states of even-leg ladder systems at half-filling, which have only a short-range magnetic order and an unbroken translational symmetry.[3–6] The keys to this behavior are elastic umklapp scattering processes across the FS which open up a charge gap at half-filling, in addition to a spin gap caused by the pairing instability. In this paper the role of these processes in a two-dimensional system will be carefully examined.

Renormalization-group (RG) methods allow an analytical treatment and, although the one-loop approximation is in principle applicable only at weak coupling, we can hope to learn about possible instabilities at the strong to intermediate couplings that apply in the cuprates. Such methods have long been successfully applied to one-dimensional models. The first attempts[7–9] to extend this analysis to two dimensions were made shortly after the discovery of high-temperature superconductivity. They focused on the dominant role of scattering processes involving Fermi-surface regions in the vicinity of van Hove singularities.

Limiting the two-dimensional FS to just two patches reduces the problem to the flow of a small number of coupling constants which can be handled analytically. For repulsive interactions there are two possible fixed points involving flows either to weak coupling or to strong coupling. The possible relevance of the latter to the cuprates was emphasized by three of the present authors.[10] They showed that under certain conditions the local charge compressibility flowed toward zero, indicating that here too umklapp scattering opened up a local charge gap.

A proper treatment requires that the flow of interactions involving the whole two-dimensional Fermi surface be included. Already several RG investigations using a discretization of the Fermi surface into N patches with $N \lesssim 32$ have been made. Zanchi and Schulz[11] studied the RG flows of a 32-patch weak coupling Hubbard model with only nearest-neighbor (NN) hopping in the kinetic-energy term. They found a crossover between an antiferromagnetic (AF) ordered ground state to a $d_{x^2-y^2}$-paired superconducting (SC) ground state as the electron density was lowered away from half-filling. Recent, more extensive, results by Halboth and Metzner[12] largely confirmed the Zanchi-Schulz results, extending them to the case where there is a small next-nearest-neighbor (NNN) hopping as well, and investigating possible incommensurate AF orderings. Although in both these investigations umklapp scattering was included, the possibility of a fixed point behavior which would be similar to that of the two-leg ladder was not explicitly considered.

In this paper we will use a one-loop RG method with a discretization of the FS into N patches ($N=32-96$) to examine the flow of the coupling constants and susceptibilities under various starting conditions. Throughout we take a substantial value for the NNN hopping amplitude, t'. On the one hand this is a realistic value for the cuprates. Second, it moves the critical density, where the saddle points are at the FS, away from half-filling so that the saddle point effects are not mixed with nesting effects on the zone diagonals, as occurs when one sets $t' \equiv 0$. When t' is substantial, one can distinguish three density regions. The simplest is the strongly

doped region where the saddle points lie above the Fermi energy, and umklapp scattering is unimportant. Here the leading instability is to *d*-wave SC—a form of Kohn-Luttinger instability, in agreement with previous studies. We call this the *d-wave-dominated regime*. A second relatively straightforward density regime is the weak doping regime close to half-filling, where the approximate nesting of FS segments near the zone diagonals dominates, and an AF instability is favored—again in agreement with previous studies. We call this region the *approximate nesting regime*.

The intermediate regime is most interesting and will be the focus of this work. In this case the saddle points lie slightly below the Fermi energy and umklapp processes involving these FS regions are highly relevant. We call this density region the *saddle-point regime*. As in the case of the half-filled two-leg ladder, these umklapp processes, which strongly drive the AF fluctuations, act to reinforce *d*-wave pairing so that this channel competes strongly with the AF tendencies. If one looks only at these two instabilities in the one-loop RG, it is not possible to decide which dominates. In the case of the two-leg ladder the uniform (Pauli) spin susceptibility flows to zero, indicating singlet pairing in the true ground state—a result confirmed when bosonization methods are used to examine the strong coupling state below the critical scale in the one-loop scheme. Similarly in the present two-dimensional case we find that an examination of the uniform spin susceptibility favors an assignment of the strong-coupling fixed point to the class of the two-leg ladder. Further, the local charge compressibility defined for these FS segments also appears to scale to zero, just as in the half-filled two-leg ladder. We also note that the unusual RG flow in both the half-filled two-leg ladder and in the saddle point regime of the two-dimensional (2D) model can be understood as arising from a mutual reinforcement of *d*-wave and umklapp processes (see Sec. III), it is therefore not restricted to quasi-1D systems. Below (Sec. VIII) we present a detailed examination of this saddle-point regime. We argue that rather than the simple crossover between *d*-wave SC and AF order as the density varies, found by previous authors, an interpretation in terms of the formation of an insulating spin liquid (ISL), which truncates the FS segments near the saddle points, is more appropriate. Although we do not have a theory of the strong-coupling phase, and therefore alternative interpretations cannot be ruled out, all information extracted from the one-loop flow is consistent with our proposal. The ISL can be viewed as a form of *d*-wave RVB (resonance valence bond) state as in the case of the two-leg ladder. Such a state represents a clear violation of the Landau theory which does not rely upon a translational symmetry breaking mechanism.

Clearly an instability that partially truncates the Fermi surface with a charge gap can be seen as a forerunner of the Mott insulating state which occurs for intermediate to strong interactions. Since our motivation is to understand better the phase diagram of the high-T_c cuprates, we are most interested in such instabilities. However, we are aware that there are other instabilities which appear in a weak coupling theory driven by the diverging density of states (DOS) at the van Hove points. These are the Stoner instability to ferromagnetism and, as remarked by Halboth and Metzner,[12] the Labbé-Friedel or Pomeranchuck instability from square to rectangular symmetry. These split the saddle points when the Fermi energy lies near the van Hove singularity. This is a drawback of using a weak-coupling approach to describe an intermediate to strong coupling problem. We will simply ignore these DOS-related instabilities in the forward scattering channel, and concentrate on those which we believe are more relevant as weak-coupling signatures of the intermediate to strong coupling problem.

Finally, a defect of our one-loop approximation is that it does not lead to a description of the strong-coupling phase of the system which it predicts. There are many approaches in the literature which attempt to construct a theory of such a state that we can loosely call a lightly doped *d*-wave RVB state.[1,5,13–15] Our aim here is rather different, and seeks to complement these strong-coupling theories by examining the approach from the strongly overdoped regime which behaves as a conventional Landau-Fermi liquid with an instability toward weak-coupling *d*-wave superconductivity. The question we seek to address is the form of the instability in a Landau-Fermi liquid which leads to this doped RVB state. How does it differ from a simple *d*-wave superconducting instability, and how does the proximity to the Mott insulating state at half-filling manifest itself?

II. MODEL AND ITS FERMI SURFACE

The kinetic energy of the t-t' Hubbard model is given by the tight-binding dispersion

$$\epsilon(\mathbf{k}) = -2t(\cos k_x + \cos k_y) + 4t' \cos k_x \cos k_y - \mu \quad (1)$$

with NN hopping t, NNN hopping t', and chemical potential μ. Typically we choose $t' = 0.3t$, which yields a small convex curvature of the FS around (π,π) at higher fillings. Another essential curve is the umklapp surface (US) which connects the van Hove points with straight lines. If the FS crosses this line, two particles at the FS can be scattered from one side of the US to the opposite one in an elastic process. As we will see, these additional scattering channels then enhance the scale of the transition to a strong-coupling regime.

The initial interaction is taken to be a simple on-site repulsion

$$H_U = U \sum_{\mathbf{x}} n_{\mathbf{x},\uparrow} n_{\mathbf{x},\downarrow}, \quad (2)$$

which is constant in k space. The effective interaction will develop a pronounced k-space structure in the RG flow.

In recent years there have been several RG approaches to the 2D Hubbard model. Schulz[8] and Lederer, Montambaux, and Poilblanc[9] studied the RG flow of the processes connecting the saddle points emphasizing the divergence of both AF and *d*-wave pairing correlations. Dzyaloshinkii[7] discussed the weak coupling non-Fermi-liquid fixed point of such a model. Similar studies were made by Alvarez *et al.*[16] and Gonzalez *et al.*[17] Later on, in a related formalism based on parquet equations, the authors of Ref. 18 examined the interplay between critical scales and effects of the FS curvature

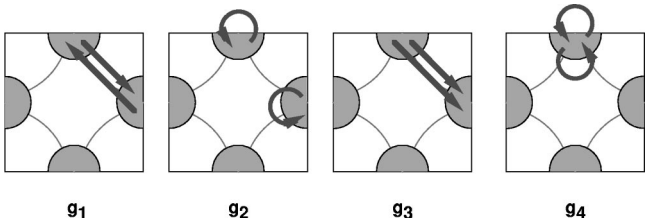

FIG. 1. The relevant scattering processes in the two-patch model. The gray semicircles denote the phase-space patches around the saddle points. The interactions are assumed to be spin independent and constant over the patches. In this notation the spins of the initial and final particles connected by an arrow have to be the same.

for a quasi-2D model restricted to approximately flat FS faces close to half-filling. Another study of nesting effects between flat FS segments was given by Vistulo de Abreu and Doucot.[19] Zanchi and Schulz[11] presented the first fully two-dimensional treatment, based on Polchinski's RG equation. They studied the 2D Hubbard model with $t'=0$, and found two different regimes with dominant AF in the one and d-wave pairing correlations in the other. A more detailed analysis of the leading instabilities was given by Halboth and Metzner[12] using RG equations for Wick ordered functions.[20] In this paper we study the RG flow for the one-particle irreducible (1PI) vertex functions for the model given by Eqs. (1) and (2), to investigate the possibility of a strong-coupling phase which is a precursor of the Mott insulating state, as suggested by the two-patch study of Ref. 10. A brief account of the RG technique we use here is given in Appendix A.

III. TWO-PATCH MODEL REVISITED

We start with a brief discussion of the dominant mechanisms for the case where the FS is at the saddle points. These are most transparent in the two-patch model,[10,8,9] where only small phase-space patches around the saddle points at $(\pi,0)$ and $(0,\pi)$ are kept. Neglecting a possible frequency dependence, we can approximately describe the scattering processes within and between the two patches by four coupling constants, $g_1,\ldots,g_4$, depicted in Fig. 1.

The main terms which drive the one-loop RG flow of these vertices are (a) the particle-particle loop d_0 with zero total incoming momentum, which diverges like $\log^2(\Lambda_0/\Lambda)$ with decreasing energy scale $\Lambda \leqslant \Lambda_0$ due to the van Hove singularity in the density of states; and (b) the particle-hole loop with momentum transfer (π,π) denoted by d_1, which, in the presence of a small but nonzero t', diverges like $\log(\Lambda_0/\Lambda)$ with a large prefactor.[21] Keeping only these two contributions, and denoting $y=\log(\Lambda_0/\Lambda)$, so that decreasing Λ means increasing y, we obtain the RG flow equations

$$\dot{g}_1 = 2\dot{d}_1 g_1 (g_2 - g_1), \tag{3}$$

$$\dot{g}_2 = \dot{d}_1 (g_2^2 + g_3^2). \tag{4}$$

$$\dot{g}_3 = -2\dot{d}_0 g_3 g_4 + 2\dot{d}_1 g_3 (2g_2 - g_1), \tag{5}$$

$$\dot{g}_4 = -\dot{d}_0 (g_3^2 + g_4^2). \tag{6}$$

where $\dot{g}_i = \partial g_i / \partial y$, and $\dot{d}_0, \dot{d}_1 \geqslant 0$. It is useful to briefly review the analysis of the two-patch model of Ref. 10. The second term on the right-hand side of Eq. (5) enhances the basin of attraction of the strong-coupling fixed point. Starting from the onsite repulsion $g_1=g_2=g_3=g_4=U$ given by Eq. (2), the coupling constants diverge at a scale Λ_c: $g_3 \to +\infty$, $g_4 \to -\infty$, and $g_2 \to +\infty$; g_1 diverges more slowly. Initially there is a competition between the two terms on the right-hand side of Eq. (5), but the right-hand side of Eq. (6) is always negative, and thus decreases g_4. Eventually, g_4 becomes negative; then both terms in Eq. (5) have the same sign, which accelerates the flow to strong coupling.

For incoming and outgoing particles directly at the saddle points g_3 processes correspond to both Cooper and umklapp processes. However, away from the saddle points we can distinguish between Cooper processes with approximately zero total incoming momentum driven through the particle-particle channel and umklapp processes with momentum transfer $\approx(\pi,\pi)$ driven by the corresponding particle-hole channel. From this point of view, Eq. (5) states that for incoming and outgoing wave vectors near the saddle points the umklapp and the $d_{x^2-y^2}$-wave Cooper channel are coupled, and mutually reinforce each other through the g_3 and g_4 processes which belong to both channels, thereby increasing the critical scale Λ_c. In fact the divergence of the umklapp scatterings processes implies a divergence of the d-wave couplings, and vice versa.

An analysis of the susceptibilities shows a competition between divergences in the $d_{x^2-y^2}$ pairing and the AF channel controlled by the flow of the combinations g_3-g_4 and g_2+g_3, respectively. In this case of competing singularities it is not clear cut which of them dominates. Furukawa, Rice, and Salmhofer proposed to resolve the issue by examining the uniform spin susceptibility and the charge compressibility. For not-too-weak values of U/t and t'/t they found that both are driven to zero by the pairing and umklapp processes, respectively. On this basis they assigned the fixed point to be in the same class as that of the repulsive two-leg ladder at half-filling. In that system, the one-loop RG also exhibits competing and equally strong divergences in the d-wave pairing and AF channels, but the ground state is known to be an insulating spin liquid from a bosonization treatment of the strong-coupling regime.[4,5] This form of ground state is already signaled in the RG calculation by the suppression toward zero in the uniform spin susceptibility and the charge compressibility. The ISL in the two-leg ladder at half-filling is a form of RVB state with an approximate d-wave pairing symmetry, but without any explicit translational or gauge symmetry breaking.

IV. TECHNIQUE

For the N-patch analysis we use a Wilson RG flow for 1PI vertex functions. The full RG flow associates with every energy scale Λ below the bandwidth Λ_0 an effective interaction for the particles with energies $\epsilon(\mathbf{k})$ below Λ, in a way that the generating functional for the Green functions remains

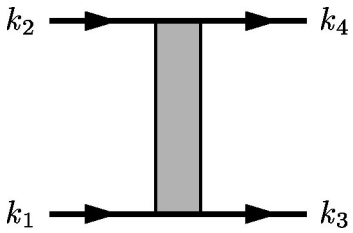

FIG. 2. The vertex corresponding to $V_\Lambda(\mathbf{k}_1,\mathbf{k}_2,\mathbf{k}_3)$.

independent of the scale Λ. Because of this exact invariance, the effective interaction is no longer just quartic but an infinite power series in the fields. The full RG can be expressed as an infinite hierarchy of differential equations for the 1PI m-point vertex functions. Here we study a truncation of this infinite system in which only the two- and four-point functions are kept. A derivation of the full flow equations is given in Appendix A. Here we just state the results, which are rather simple. Because our model is two dimensional, continuous symmetries cannot be broken by long-range order at any positive temperature. Therefore, the effective action must be gauge invariant and invariant under spin rotations, hence the four-point function is determined by the function $V_\Lambda(\omega_1,\mathbf{k}_1,\omega_2,\mathbf{k}_2,\omega_3,\mathbf{k}_3)$ which describes the scattering of two incoming particles $(\omega_1,\mathbf{k}_1,\sigma_1)$ and $(\omega_2,\mathbf{k}_2,\sigma_2)$ into two outgoing particles $(\omega_3,\mathbf{k}_3,\sigma_3)$ and $(\omega_4,\mathbf{k}_4,\sigma_4)$, where $\sigma_1=\sigma_3$, $\sigma_2=\sigma_4$, and $\omega_4=\omega_1+\omega_2-\omega_3$, and $\mathbf{k}_4$ is given by momentum conservation as $\mathbf{k}_4=\mathbf{k}_1+\mathbf{k}_2-\mathbf{k}_3$ modulo reciprocal-lattice vectors. Because the spin of particle 1 (first incoming) is the same as that of particle 3 (first outgoing), and similarly for particles 2 and 4, we may draw the vertex corresponding to V_Λ as in Fig. 2, where the solid fermion lines going through at the top and bottom of the vertex indicate that spin is conserved along these lines.

The contributions to the right hand side of $\dot{V}_\Lambda = (\partial/\partial\Lambda)V_\Lambda$ can then be represented graphically as in Fig. 3. In these graphs, one of the internal lines represents a full electron propagator

$$G_\Lambda(\mathbf{k},i\omega_n)=\frac{\chi_\Lambda(\mathbf{k})}{i\omega_n-\epsilon(\mathbf{k})-\chi_\Lambda(\mathbf{k})\Sigma_\Lambda(\mathbf{k},i\omega_n)}, \qquad (7)$$

where $\chi_\Lambda(\mathbf{k})=1-\{\exp[(|\epsilon|-\Lambda)/(0.05\Lambda)]+1\}^{-1}$ cuts off energies below Λ. The other line stands for a single-scale propagator

$$S_\Lambda(\mathbf{k},i\omega_n)=\frac{\dot{\chi}_\Lambda(\mathbf{k})[i\omega_n-\epsilon(\mathbf{k})]}{[i\omega_n-\epsilon(\mathbf{k})-\chi_\Lambda(\mathbf{k})\Sigma_\Lambda(\mathbf{k},i\omega_n)]^2}. \qquad (8)$$

Because it contains the derivative of the cutoff function with respect to Λ, S_Λ is nonzero only at energies close to Λ. Since there are two possibilities for assigning G_Λ and S_Λ to the internal lines, each graph stands for two contributions. Apart from that the usual diagrammatic rules hold: the graph with the fermion loop receives a factor 2 from the spin trace and a minus sign.

The contributions to the self-energy have a graphical representation shown in Fig. 4. Here the internal line stands for a single-scale propagator S_Λ.

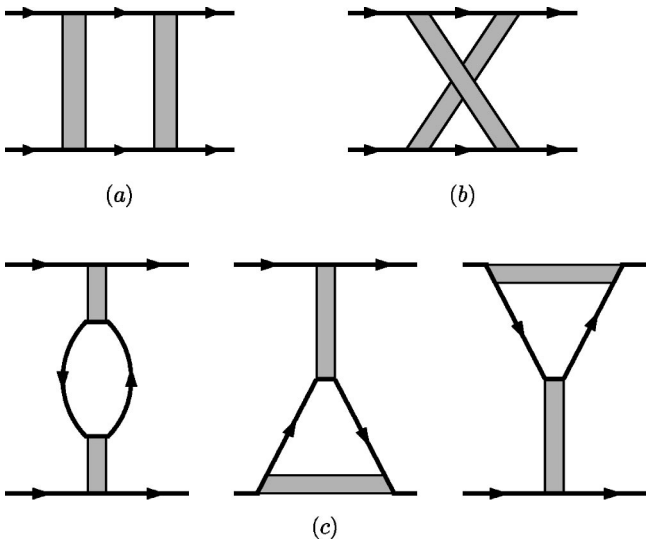

FIG. 3. The contributions to the right-hand side of the RGDE. (a) The particle-particle term. (b) The crossed particle-hole term. (c) The direct particle-hole terms. The first of these three graphs receives a factor -2 because of the fermion loop.

In the main part of this paper we will neglect self-energy corrections to the propagator. Then $G(i\omega_n,\mathbf{k})=\chi_\Lambda(\mathbf{k})[i\omega_n-\epsilon(\mathbf{k})]^{-1}$, and the single scale propagator is simply $S_\Lambda=\partial G_\Lambda/\partial\Lambda$. In Appendix A we show some results for a flow with the real part of the self-energy on the FS taken into account. A more complete study including self-energy effects, in particular the effects of the wave-function renormalization, is underway.

We want to emphasize that our RG method does not rely on any form of scale invariance or scaling *Ansätze*. The RG we set up in Appendix A provides an exact rewriting of the generating functional in terms of the effective action. The approximations we make in the present paper are (i) we discard the 1PI m-point functions with $m\geqslant 6$, (ii) we project the four-point function to the Fermi surface and frequency zero (see Sec. VI), and (iii) we neglect the self-energy corrections. We discussed the justification of (i) and (ii) in detail in Ref. 22. The justification for (ii) is a standard RG argument, and the full momentum dependence can in principle be reconstructed by calculating susceptibilities and related quantities. The justification of (i) is less trivial, but possible for curved Fermi surfaces and in a specific scale range.[22] (iii) is an approximation on which we shall improve in a further paper.

In systems with a Cooper instability, the flow always tends toward strong coupling at a sufficiently low scale. This happens even in repulsive systems because of the Kohn-Luttinger effect. However, in repulsive systems, and initially weakly coupled systems, the flow stays in the weak-coupling

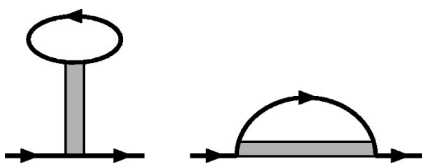

FIG. 4. The contributions to the self-energy.

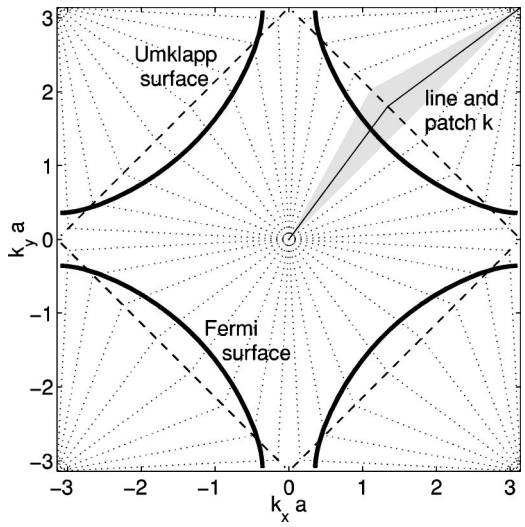

FIG. 5. The Brillouin zone, Fermi, and umklapp surfaces, and the lines in the patch centers for $N=32$.

regime down to a very low scale which may never be reached because the temperature, which acts as a natural infrared cutoff, stops the flow before that (in the usual Kohn-Luttinger effect, this scale is at most of order $e^{-\text{const}/U^2}$; see Refs. 23 and 24). In this case the system stays weakly coupled above a certain temperature, and components of the Fermi surface limits of the four-point function can be identified with the Landau interaction function $f(\mathbf{k},\mathbf{k}')$.[25,26]

When the four-point function flows to strong coupling, the critical scale Λ_c where the coupling constants diverge gives an estimate for the scale where the quasiparticles will be strongly modified or entirely destroyed (e.g., for the superconducting transition, a gap opens up) (see Fig. 5). The general picture we find in this model is that the flow always tends to strong coupling, but that for fillings where umklapp scattering is favored by the geometry of the Fermi surface, the critical scale is strongly enhanced.

We note that in our RG method the temperature T is retained as a physical parameter, and that the RG procedure of decreasing the scale Λ is *a priori* not related to changing the temperature. The four-point vertex at scale Λ is the effective interaction for the modes with energy below Λ, and at the same time it is the four-point function with infrared cutoff Λ. For $\Lambda \ll T$, one should use the second interpretation. Note that because we do not impose a scale-dependent cutoff on the frequencies, the flow does not stop exactly at the point when Λ decreases below the smallest fermionic Matsubara frequency, $\omega_1=\pi T$.

V. NUMERICAL IMPLEMENTATION

Next we describe the practical implementation of this RG scheme for the 2D Hubbard model. First we define a phase space discretization following Zanchi and Schulz.[11] The idea is to discretize the Brillouin zone (BZ) into N segments centered around N lines. Each line with index $k \in \{1,\ldots,N\}$ starts from the origin (Γ point) in a certain angular direction and from the Y point $(\pm\pi,\pm\pi)$, so that the lines meet at the umklapp surface. All phase-space integrations with measure $d^2k/(2\pi)^2$ are performed approximately as sums over the lines and integrations over the radial direction. These imply Jacobians for polar coordinates with respect to the Γ or Y point, respectively. The interaction vertex $V_\Lambda(\mathbf{k}_1,\mathbf{k}_2,\mathbf{k}_3)$ depends on two incoming wave vectors $\mathbf{k}_1$ and $\mathbf{k}_2$ and one outgoing wave vector $\mathbf{k}_3$ lying in segments k_1, k_2, and k_3, respectively (here we have already projected the frequencies to zero). The fourth wave vector $\mathbf{k}_4$ is fixed by momentum conservation. In a next approximation we select a large but finite number of coupling constants representative for certain regions in the space spanned by $\mathbf{k}_1$, $\mathbf{k}_2$, and $\mathbf{k}_3$.[27] We choose to take these wave vectors as the crossing points of the lines k_1, k_2, and k_3 with the Fermi surface, i.e., $\mathbf{k}_F(k_1)$, $\mathbf{k}_F(k_2)$, and $\mathbf{k}_F(k_3)$, which lie at the centers of the corresponding FS patches. By Taylor expansion and power counting arguments,[22] the leading part of the flow is given by the coupling functions on the Fermi surface and at zero frequency. Thus we approximate[28] the function $V_\Lambda(\mathbf{k}_1,\mathbf{k}_2,\mathbf{k}_3)$ by $V_\Lambda[\mathbf{k}_F(k_1),\mathbf{k}_F(k_2),\mathbf{k}_F(k_3)]=V_\Lambda(k_1,k_2,k_3)$ for all wave vectors $\mathbf{k}_i$ in the same patch k_i, where $i=1$, 2, and 3.

VI. PARAMETERS

The initial condition for the flow of the couplings is given by Hubbard interactions $V_{\Lambda_0}(k_1,k_2,k_3)=U$. For most results discussed here, we take $U=3t$. We choose this rather strong initial interaction because we are interested in the breakdown of the Landau-Fermi liquid due to interaction effects, and do not aim at a classification of possible weak-coupling instabilities. For all results shown here, $t'=0.3t$, which is in the range of the values reported for the cuprates.

We will vary mainly the temperature T and the particle density near and below half-filling via the chemical potential μ. We considered values between $\mu=-0.7t$ and $\mu=-1.35t$ which correspond to fillings between $\approx$99% and $\approx$62% of half-filling. The van Hove filling, where the FS exactly touches the saddle points, is given by $\mu=-4t'=-1.2t$.

For a given μ the dependence of the average particle number on T is weak, and irrelevant for the results. Both parameters μ and T change the effective phase space for the various scattering processes. In particular, increased temperature provides a larger phase space for particle-hole processes with momentum transfer (π,π), which play an important role. This is similar to the quasi-1D organic conductors where above a certain temperature the band curvature due to interchain hopping becomes irrelevant, and 1D nesting effects determine the behavior of the system.[29]

We integrate the RG equations with decreasing energy scale Λ starting from an initial scale $\Lambda_0 \approx 4t$. Typically, we observe a flow to strong coupling where at least some coupling constants take large positive or negative values. We define the critical scale Λ_c as the scale where the first coupling reaches a high absolute value like $50t$. Further we introduce a critical temperature T_c above which $\Lambda_c=0$ (see Fig. 13).

The analysis of the divergence of the coupling functions yields information on the true strong-coupling state as the

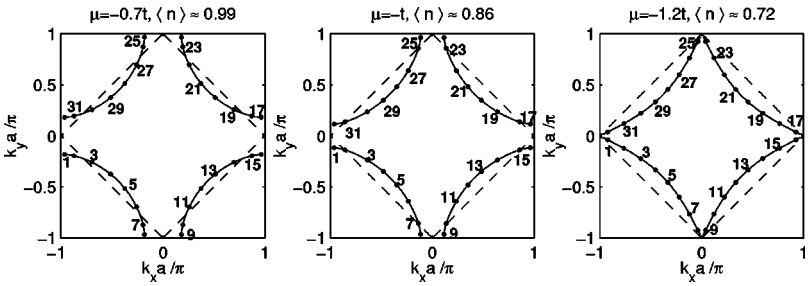

FIG. 6. Fermi surfaces and the 32 points for the three different chemical potentials discussed in the text. $\langle n \rangle$ denotes the average particle number per site, i.e., $\langle n \rangle = 1$ corresponds to half-filling. The dots on the FS (solid line) indicate the patch centers, with patch indices given by the numbers. The dashed line denotes the umklapp surface (US).

interaction processes growing most strongly in the RG flow represent the dominant terms in the Hamiltonian which determines the low-energy physics. We choose to analyze the flow to strong coupling at scale Λ_W where the coupling functions just exceed the order of the bare bandwidth, i.e., at $V_{\Lambda_W,\max} \approx (8-12)t$. At these scales, and for typical temperatures, the coupling functions have already developed a pronounced **k**-space structure and the dominant interaction terms at that scale will certainly be important for the strong-coupling state. On the other hand, the FS shift due to one-loop self-energy corrections is still small (see Appendix C), such that it does not qualitatively change the flow above Λ_W. Similarly the scattering rate for particles at the FS (obtained from an approximative RG calculation of the two-loop self-energy[30]) remains smaller than Λ_W. Note, however, that at Λ_W and for initial interaction $U=3t$ the flow has not reached an asymptotic form, and different classes of coupling constants would evolve differently if we continued the flow below Λ_W (where our method breaks down). Therefore, the analysis of the flow to strong coupling remains qualitative, and does not provide definitive conclusions about the true strong-coupling state.

VII. COUPLINGS AND SUSCEPTIBILITIES

We will discuss the results of our numerical RG scheme by analyzing the interaction on the FS and susceptibilities. In the flow to strong coupling we will identify the most relevant, i.e., divergent couplings. In the absence of scale invariance we cannot expect to obtain simple expressions for the form of their divergence; therefore, we use their numerical values as a function of the scale to make a qualitative comparison.

Along with the interactions we calculate the *d*-wave pairing susceptibility χ_{dw} for zero pair momentum, and the spin susceptibility $\chi_s(\mathbf{q})$ around $\mathbf{q}=(\pi,\pi)$. The method we use is again described in Appendix A. Typically both χ_{dw} and $\chi_s(\mathbf{q})$ grow strongly as the interactions flow to strong coupling. In general the ratio of these susceptibilities is a complicated, nonmonotonic, function of the scale. Therefore, we do not attempt to draw sharp boundaries between different cases.

As discussed earlier in Sec. I, it is often useful also to analyze the coupling to uniform external charge and spin fields given by

$$H_{c/s} = \int \frac{d\mathbf{k}}{(2\pi)^2} h_{c/s}(\mathbf{k})(c^\dagger_{\vec{k},\uparrow} c_{\vec{k},\uparrow} \pm c^\dagger_{\vec{k},\downarrow} c_{\vec{k},\downarrow}),$$

where the subscripts *c* and *s* stand for charge and spin, respectively. The **k**-independent bare couplings $h^0_{c/s}$ develop a *k* dependence due to vertex renormalizations depending on **k** leading to dressed vertex functions $h_{c/s}(\mathbf{k})$. We cannot directly incorporate these renormalizations of the uniform external fields into our present RG scheme with an infrared (IR) cutoff, as they involve only excitations in a low-energy region of width *T* around the FS. Therefore, we calculate $h_{c/s}(\mathbf{k})$ using the random-phase approximations (RPA) for the effective theory below the IR cutoff Λ. This means that we use the scale-dependent interactions $V_\Lambda(\mathbf{k}_1,\mathbf{k}_2,\mathbf{k}_3)$ in the one-loop vertex corrections for the external couplings, which then can be summed up and solved for $h_{c/s}(\mathbf{k},\Lambda)$ (see Appendix B). Note, however, that due to the use of the renormalized interactions this scheme goes beyond the normal RPA. Although it implies a further approximation, it gives a qualitatively correct description of the uniform susceptibilities in one-dimensional examples, in agreement with bosonization.[30]

VIII. RESULTS: THREE REGIMES

In the density range we examined, we always found a flow toward strong coupling at sufficiently low temperature. This gives a clear indication that the low-energy single-particle excitations of the noninteracting Hamiltonian will be strongly modified or entirely destroyed by the interactions.

The character of the flow to strong coupling varies continuously with density and temperature. However, we can identify three qualitatively different regimes, which we will call the *d-wave-dominated regime*, the *saddle-point regime*, and the *approximate nesting regime*, as illustrated in Fig. 13. For reasons mentioned above, our analysis does not allow us to draw sharp boundaries between the different regions. Rather, the character of the strong-coupling flow changes in a crossoverlike fashion as one moves from one region into the other.

In order to show the main features, we examine the flow for three densities typical for each regime. The Fermi surfaces and locations of the patch centers that label our coupling constants are displayed in Fig. 6. In Figs. 7 and 8 we show snapshots of the couplings at the scale where the largest couplings have exceeded the order of the bandwidth: we plot the dependence of the coupling $V_\Lambda(k_1,k_2,k_3)$ with the first outgoing wave vector k_3 fixed at point 1 closest to the saddle points or at point 3 closer to the BZ diagonal. In Fig. 9 we compare the flow of several relevant couplings as a function the RG scale, and in Fig. 10 we plot the behavior of

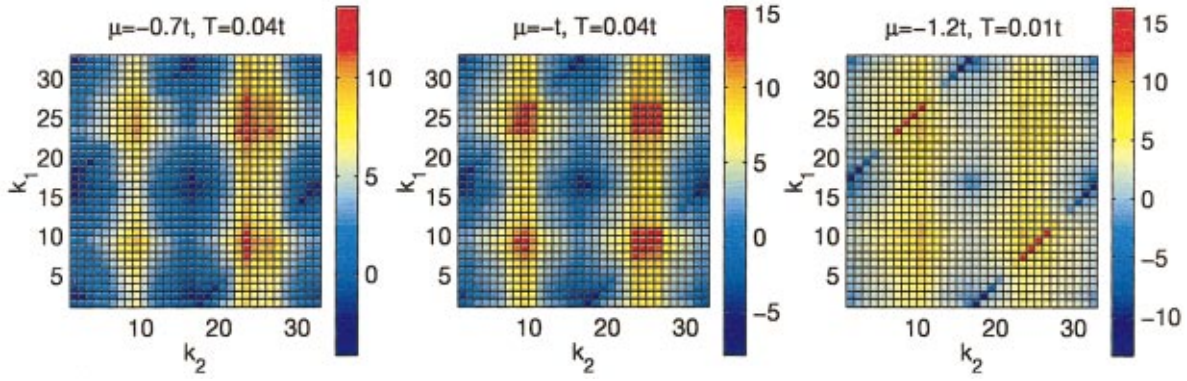

FIG. 7. (Color) Snapshot of the couplings $V_\Lambda(k_1,k_2,k_3)$ with the first outgoing wave vector k_3 fixed at point 1 (see Fig. 6) when the largest couplings have exceeded the order of the bandwidth for the three different choices of chemical potential and temperature discussed in the text. The colorbars indicate the values of the couplings.

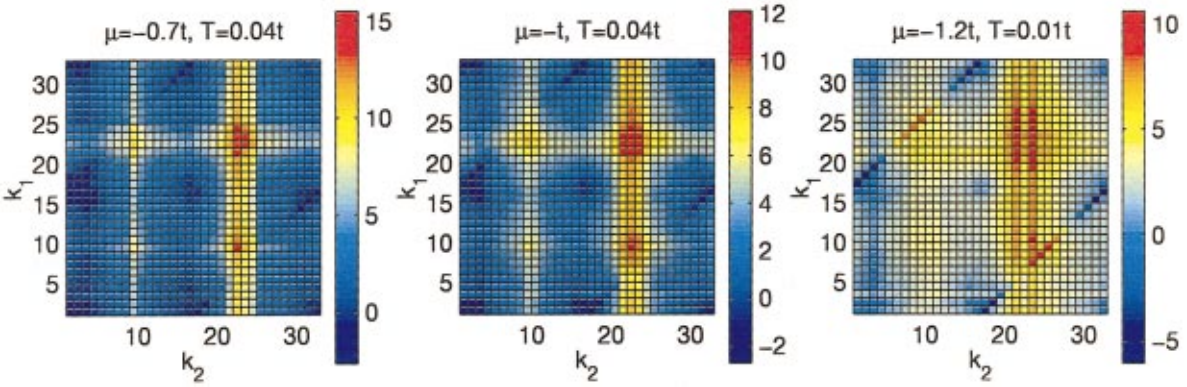

FIG. 8. (Color) Snapshot of the couplings $V_\Lambda(k_1,k_2,k_3)$ with the first outgoing wave vector k_3 fixed at point 3 (see Fig. 6) when the largest couplings have exceeded the order of the bandwidth for the three different choices of chemical potential and temperature discussed in the text. The colorbars indicate the values of the couplings. For $k_2=22$, $\mathbf{k}_2-\mathbf{k}_3\approx(\pi,\pi)$ for $\mathbf{k}_2$ and $\mathbf{k}_3$ close to the US.

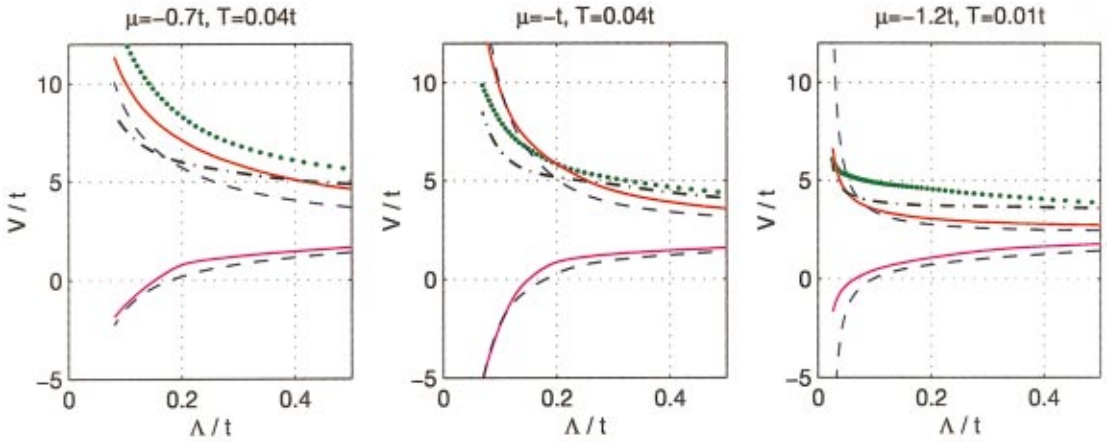

FIG. 9. (Color) Flow of the couplings for 32-patch system: *d*-wave Cooper coupling (blue dashed lines), g_3 umklapp coupling [e.g., $V_\Lambda(24,24,1)$ and $V_\Lambda(23,23,2)$; solid red lines], g_2 forward coupling [e.g., $V_\Lambda(24,1,24)$ and $V_\Lambda(23,2,23)$; black dashed dotted lines], and g_4 umklapp couplings [e.g., $V_\Lambda(16,17,1)$; solid violet lines] and umklapp scatterings $V_\Lambda(21,21,4)$ in the BZ diagonal (green) for the three different choices of chemical potential and temperature discussed in the text.

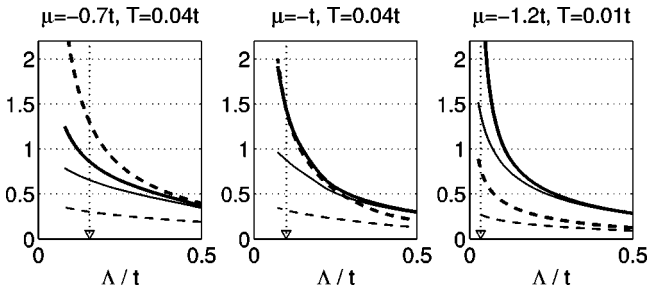

FIG. 10. *d*-wave (heavy solid line) and AF susceptibility (heavy dashed line) for the three different choices of chemical potential and temperature discussed in the text. The thin lines denote the flow of the bare susceptibilities without vertex corrections. The mark at the Λ axis indicates the scale, where the largest coupling reaches $10t$.

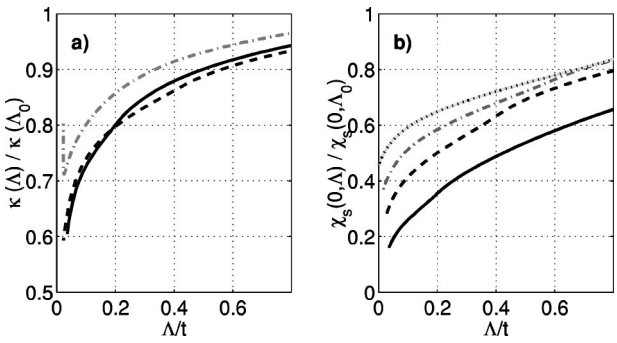

FIG. 11. (a) Flow of the charge compressibility κ normalized to their value at the initial scale $\Lambda_0=4t$ for $\mu=-1.2t$ (dashed dotted line), $\mu=-t$ (solid line), and $\mu=-0.8t$ (dashed line). (b) Flow of the uniform spin susceptibilities normalized to their initial values for $\mu=-t$ (solid line), $\mu=-0.8t$ (dashed line), $\mu=-0.6t$ (dashed-dotted line), and $\mu=-0.4t$ (dotted line). For increasing electron density, $\chi_s(0,\Lambda)/\chi_s(0,\Lambda_0)$ is less suppressed at low scales. For all curves, $T=0.04t$.

the *d*-wave pairing susceptibility χ_{dw} and the AF susceptibility $\chi_s(\pi,\pi)$. In the following we describe the three regimes in detail.

(a) The d-wave-dominated regime: At band fillings around the van Hove filling $\mu=-1.2t$ and low temperature $T=0.01t$ (see the right plots in Figs. 7, 8, and 9), the divergence of the coupling functions only occurs at a low scale, and the *d*-wave pair scatterings are by far the most strongly divergent couplings. In Fig. 7, they appear as red and blue features along the lines with patch numbers $|k_1-k_2|=N/2$ (on these lines, the incoming pair momentum is zero). Other couplings like umklapp and forward scatterings (the red, violet, and black lines in Fig. 9), grow too, but are much smaller than the Cooper couplings. This is the typical flow to strong coupling in the lightly shaded regions in Fig. 13. At low temperatures this also extends to densities slightly higher than the van Hove density.

A closer analysis shows that the *d*-wave component in the pair scattering is generated at intermediate scales by the particle-hole processes with momentum transfer (π,π) corresponding to the second term in Eq. (5). This type of flow to strong coupling can be considered as a Kohn-Luttinger-type Cooper instability, where the repulsive scattering in the particle-hole between the saddle points first generates a sizable initial value for the *d*-wave pair scattering, and is then gradually cut off at lower scales because the phase space for the (π,π) particle-hole processes decreases due to the shape of the FS. The dominance of the *d*-wave Cooper scattering is also seen in the comparison of the susceptibilities: the *d*-wave pairing susceptibility χ_{dw} grows much faster than the AF susceptibility $\chi_s(\mathbf{q})$ (see Fig. 10).

The uniform charge susceptibility κ is somewhat suppressed at intermediate scales, but very close to the instability the attractive Cooper scatterings in the forward-scattering channel start to dominate the vertex corrections to the charge coupling and cause a pole in the RPA-like expression [see Eq. (B1)] for $h_c(\mathbf{k})$ for $\mathbf{k}$ near the saddle points. This is then the reason of a sharp upturn in κ (see Fig. 11), as also observed by Halboth and Metzner.[12] At low scales the uniform spin susceptibility $\chi_s(0)$ is suppressed to zero by the strong attractive g_4 couplings favoring singlet formation. However at higher scales, which are not related to the flow to strong coupling, the naive Stoner criterion for ferromagnetism is fulfilled due the large DOS around the van Hove filling. As discussed in Sec. I we ignore this effect.

(b) The saddle-point regime: Next we increase the temperature to $T=0.04t$, and choose a band filling slightly above the van Hove filling such that the FS crosses the US (chemical potential $\mu=-t$). Now the scale where the couplings reach the order of the bandwidth is strongly enhanced. In Fig. 7 we observe that next to the *d*-wave pair scatterings additional features have developed. The strongly repulsive interactions, for instance $(k_1,k_2)\approx(24,25)\rightarrow(k_3,k_4)\approx(1,17)$, correspond to g_3-type umklapp scatterings which now diverge together with the repulsive Cooper couplings. Forward scatterings of g_2 type also show a strong increase toward the divergence. In addition, there is a general increase for couplings with momentum transfer (π,π) due to the enhanced influence of the particle-hole channel with this momentum transfer. On the other hand, we also observe strongly attractive couplings emerging, e.g., $(k_1,k_2)\approx(16,17)\rightarrow(k_3,k_4)\approx(1,18)$. These processes correspond to umklapp g_4 processes of pairs with both incoming particles at the same saddle point, and outgoing particles on opposite sides of the FS. Since these pairs have a small total momentum they couple into the Cooper channel, and are driven to strong attraction along with the attractive Cooper couplings with zero pair momentum. This clearly demonstrates that umklapp and Cooper channel are strongly coupled. For this choice of parameters the AF susceptibility grows considerably toward the divergence, and is as large as the *d*-wave pairing susceptibility.

We call this the *saddle-point regime* because the flow to strong coupling is dominated by the saddle-point regions. Here, as we will show, we find the key signatures of the ISI, and the basic mechanism of the two-patch model described in Sec. III is at work: the diverging g_3-type umklapp scattering between the saddle-point regions drives the forward scattering of g_2 type to strong repulsion; correspondingly the coupling $h_c(\mathbf{k})$ of external charge fields to these FS parts, and thus their contribution to the charge compressibility κ is increasingly suppressed as we approach the instability. This

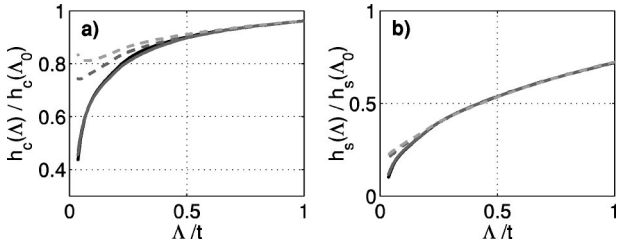

FIG. 12. Change of the charge $h_c(\mathbf{k})$ [left plot (a)] and spin couplings $h_s(\mathbf{k})$ (b) normalized to their initial values of quasiparticles with wave vector $\mathbf{k}$ on the FS as the electronic interactions flow to strong coupling from a 96-point calculation at $\mu=-t$ and $T=0.04t$. The different lines are for points close to the saddle points (solid lines), and points closer to the BZ diagonal (dashed lines).

can be seen in Figs. 11 and 12. In contrast to the FS near the saddle-point regions, which tends toward compressible, i.e., insulating behavior, for $\mathbf{k}$ in the BZ diagonal the charge coupling $h_c(\mathbf{k})$ is more or less unchanged. Therefore, this is consistent with a picture where at wave vectors near $(\pi/2,\pi/2)$ gapless charge excitations remain, while near the saddle points the FS is truncated. We use this particular behavior of the $\mathbf{k}$-space local charge compressibility to define the saddle-point regime (darker gray regions in Fig. 13): Here the charge couplings around the saddle points continue to go to zero if we integrate the flow far out of the perturbative range without any indication of the upturn in κ that we

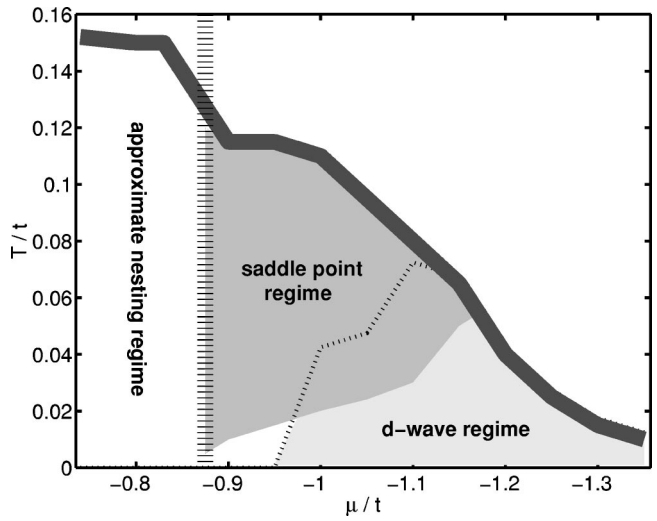

FIG. 13. Dependence of the flow to strong coupling on the chemical potential μ and temperature T for $t'=0.3t$ and an initial interaction $U=3t$. Above the thick line $\Lambda_c=0$, and we can integrate the flow down to zero scale without reaching an instability. Below the thin broken line the d-wave pairing susceptibility χ_{dw} exceeds the AF susceptibility $\chi_s(\pi,\pi)$ when the largest couplings have reached the order of the bandwidth. Above this line, $\chi_s(\pi,\pi)$ is larger than χ_{dw}. The darker gray region denotes the *saddle-point regime*, where the charge coupling of the saddle point regions goes to zero and the total charge compressibility is suppressed. The lightly shaded region represents the *d-wave-dominated regime*. Left to the thick vertical line, the instability is increasingly dominated by couplings away from the saddle points; we refer to this region as the *approximate nesting regime*.

found in the d-wave-dominated regime. However we repeat that in the flow of $V_\Lambda(k_1,k_2,k_3)$ the border between saddle-point and d-wave-dominated regimes is a continuous crossover.

The uniform spin susceptibility exhibits a similar, albeit somewhat more isotropic, suppression (see Figs. 11 and 12) when we approach the instability in this saddle-point regime. On the one hand, this is plausible because the rapid growth of the d-wave susceptibility signals strong singlet pairing tendencies. On the other hand, the AF susceptibility $\chi_s(\pi,\pi)$ seems to diverge as well, from which one might expect long-range AF order, i.e., a strong-coupling state with nonzero $\chi_s(0)$.

Here we argue that for the saddle-point regime the more likely candidate is a spin liquid state with a strong short-range AF correlation but a nonzero spin gap. As explained above, the flow to strong coupling in this regime is caused by the coupling and mutual reinforcement of the d-wave pairing and the umklapp processes between the broad saddle-point regions. Therefore, the strong-coupling state should feature a singlet pairing of the d-wave channel *and* a strong enhancement of $\chi_s(\mathbf{q})$ for $\mathbf{q}\approx(\pi,\pi)$. This is exactly what we observe for χ_{dw} and $\chi_s(\mathbf{q})$. Moreover, due to the extension of the saddle-point regions, the peak of $\chi_s(\mathbf{q})$ is very broad around (π,π), and does not sharpen significantly in the flow. Therefore, we expect a rather short AF correlation length of 2–3 lattice spacings. This is in contrast to the $t'=0$ case very close to half-filling, where we find sharp peaks in $\chi_s(\mathbf{q})$ developing around $\mathbf{q}=(\pi,\pi)$ and where one would expect AF long-range order at $T=0$.

(c) The approximate nesting regime: The plots on the left in Figs. 7, 8, and 9 show the flow for a higher filling ($\mu=-0.7t$). In this case the leading interactions are umklapp couplings between the BZ regions where the FS intersects the US and in the BZ diagonals (see the red features in Fig. 8, and the green lines in the left plot in Fig. 9), while the importance of the vicinity of the saddle points decreases. We call this the *approximate nesting regime*. Here, due to the higher band filling, the dominating FS regions are now further away from the saddle points. As a consequence, the coupling between umklapp and pairing channels decreases, and the d-wave pairing processes become less relevant. This can best be seen from the weaker flow of the attractive Cooper couplings in Fig. 9. Now the AF susceptibility clearly exceeds the d-wave pairing susceptibility (Fig. 10). This signals increasing AF ordering tendencies which are in accordance with sharper (π,π) features in the interactions (see Fig. 8), decreasing suppression of $\chi_s(0)$ relative to its initial value (see Fig. 11), and a sharper peak of $\chi_s(\vec{q})$ around (π,π). The charge susceptibility is also suppressed as in the saddle-point regime; however, the FS regions with smallest charge couplings stay fixed to the US, and therefore move toward the BZ diagonal if we increase the filling.

We emphasize that in our RG treatment the next-nearest-neighbor hopping t' is important for the existence of a sizable saddle-point regime. For zero or very small t', the FS is closer to the US in the BZ diagonals, and the (π,π) scattering between the rather flat FS faces dominates even more

strongly than in our approximate nesting regime with more FS curvature. If we now decrease the band filling, at some point, as pointed out in Ref. 18, and explicitly shown for the 2D case in Ref. 11, these processes are cut off at low scales, and can only serve as generators of an attractive *d*-wave initial condition. With t' very small the system crosses rather sharply from a nesting regime into a *d*-wave-dominated regime, without going through a saddle-point regime in between. In this sense, in the saddle-point regime substantial values of t' frustrate antiferromagnetism in a twofold way: first they destroy the nesting to a large degree; and second, more interestingly, they lead to a RG flow with clear spin-gap tendencies, suggesting the formation of an ISL.

Further we repeat that the unusual flow in the saddle-point regime with the spin- and charge-gap tendencies is primarily caused by the mutual reinforcement of Cooper and umklapp processes near the saddle points. The scattering of a Cooper pair from one saddle-point region to the other involves a momentum transfer $\approx(\pi,\pi)$, and can therefore be driven by umklapp processes with the same momentum transfer, and vice versa. This coupling does not rely on the precise location or existence of the van Hove singularities. The latter merely serve to enhance the dominance of the saddle-point regions over the FS parts near the BZ diagonal, which are already less important due to their distance to the US.

Apart from the suppression of the total charge compressibility described above, there are other potential instabilities in the forward-scattering channel. For example, as pointed out by Halboth and Metzner,[12] there appears to be a strong tendency toward Labbé-Friedel or Pomeranchuck FS deformations which break the square symmetry. These are mainly rectangular deformation modes which split the degeneracy of the saddle points. However, we will ignore those tendencies for the reasons discussed above. We have checked that a moderate deformation of the FS that breaks the square symmetry and leads to saddle point splittings of the order of the critical scale $\sim 0.1t$ does not invalidate the results described above.

A difference to the two-patch analysis of Sec. III is that the saddle-point regime, where we observe the ISL signatures in our *N*-patch calculation, is found at positive temperatures and densities slightly higher than the van Hove density assumed in the two-patch analysis. The reason for the latter is that in the *N*-patch flow the FS parts away from the saddle points reinforce mainly the Cooper channel. Only if the FS really crosses the US is there sufficient low-energy phase space for the umklapp processes, which then act together with the Cooper processes, leading to an unusual strong coupling flow. For similar reasons nonzero temperature is needed for the saddle-point regime. A moderate T smears out the FS, and provides additional phase space for both particle-particle processes with small total momentum and particle-hole processes with momentum transfer (π,π). Especially due to the latter there is a certain temperature range where this thermal phase space gain outweighs the ordinary decrease of the one-loop contributions for increasing T, and the critical scale Λ_c is enhanced with respect to its $T=0$ value.

IX. DISCUSSION AND CONCLUSIONS

We have presented an *N*-patch renormalization-group analysis of the 2D Hubbard model, and found indications that the path from a Fermi-liquid-like state to the Mott insulating state may pass through a spin liquid phase with partially truncated FS and incompressible regions around the saddle points. Certainly the above results have to be interpreted with care and are only qualitative as they are an attempt to learn about possible strong-coupling states from extrapolating weak-coupling flows. However, they demonstrate that the breakdown of a Fermi liquid through an ISL state with a partially truncated FS seems to be a viable concept, because in the saddle-point regime the qualitative features of the ISL, e.g., spin and charge gaps, are visible as tendencies in our weak-coupling approach. The essential phenomenon which can be identified as the cause for the ISL in the two-patch model, namely, the coupling of umklapp and pairing channel, is also found to exist in a sizable temperature and density range in our improved RG calculation, which includes the entire Fermi surface. We believe that this behavior is robust because it only requires sufficiently large low-energy phase space around the saddle points, but does not rely on further details of the interaction or dispersion relation. What remains to be clarified is when this interplay between pairing and umklapp processes, which frustrates symmetry-breaking tendencies and thus leads to an ISL, indeed represents an energetically favorable situation for the system. Another interesting and related aspect is the question of the precise conditions for which the overlap between the channels becomes too small, such that at $T=0$ the system can still undergo a transition into a symmetry-broken state with presumably renormalized properties. In our calculation such symmetry-broken states are suggested on either side of the saddle-point regime, e.g., in the *d*-wave-dominated phase or closer to half-filling in the approximate nesting regime.

Our approach certainly bears some appealing features when compared to the high-T_c cuprates. However, note that especially very close to half-filling, in the approximate nesting regime, our description will be much too simple, as interaction effects which are not taken into account will become large. On the other hand further, away from half-filling in the saddle-point regime, we can hope to give a reasonable qualitative description of the driving forces for the breakdown of the Landau-Fermi liquid. Due to the mutual reinforcement between Cooper and umklapp channel *d*-wave pairing correlations appear in a natural way at an enhanced scale on the threshold to the Mott state. If the insulating tendencies are strong enough they will lead to ISL formation around the saddle points.

The stabilization of the ISL in the vicinity of the saddle points opens up a channel to enhance Cooper pairing on the remaining open parts of the FS. A similar mechanism was recently proposed in Ref. 31, whose authors examined a model with infinite mass preformed pairs existing at higher temperatures in the vicinity of the saddle points. Let us assume that an ISL has formed in a region (called the *A* region) around the saddle points at an energy scale Λ_{ISL}. Then the dominant coupling between the ISL and the open FS parts

(called the B regions) will occur through the exchange of zero-momentum hole pairs in the Cooper channel. Further it will occur in the d-wave pairing channel. We denote by V_{AB} the pair scattering matrix element between the ISL in the A regions and the open B regions of the FS at the scale Λ_{ISL}, and by ϵ_A the energy relative to the chemical potential to add a hole pair to the ISL. Then, at energy scales $\Lambda < \Lambda_{\mathrm{ISL},}$ an additional attraction V_{BB} is generated between pairs in the open B regions, which has a pole at

$$\Lambda_c^B = \Lambda_{\mathrm{ISL}} \exp\left(- \frac{\epsilon_A}{N_{AB}} \right), \qquad N_{AB} = n_A \int_{B\text{-FS}} \frac{dk}{(2\pi)^2} \frac{V_{AB}^2(\mathbf{k})}{v_F(\mathbf{k})}. \tag{9}$$

Here the integral is over the Fermi surface of the B regions, and n_A denotes the number of intermediate states with two additional particles in the A regions per lattice site.

Although we do not have a full theory of the strong-coupling phase, it is plausible to assume that in the A regions a charge gap spreads out along the US in analogy to ladder systems which when lightly doped show simultaneously channels with and without a charge gap.[6,32] Then the open B region of the FS will enclose an area measured from the US, determined by the hole density, and so the superfluid density will be given by the hole density in the saddle-point regime. There will also be two energy scales, a higher one determining the onset of the ISL in the A regions, and a lower scale setting the transition temperature to the superconductivity, T_c. These features are in nice qualitative agreement with the observations in the underdoped cuprates. However, a full microscopic theory of the strong-coupling phase and also the crossover to the more conventional d-wave superconductivity in the lower electron density d-wave regime remains to be worked out. Note that in the latter regime umklapp scattering is irrelevant at low-energy scales, and the superfluid density is determined by the electron density, not the hole density.

Finally we note that the ISL concept might provide a microscopic basis for understanding the angle-resolved photoemission electron spectroscopy results on the cuprates which clearly show the truncation of the FS around the saddle points,[33] and also for phenomenological models[34] which have proven to be plausible descriptions of the transport properties of the normal state of the underdoped high-T_c cuprates.

ACKNOWLEDGMENTS

We would like to thank G. Blatter, J. Feldman, D. Geshkenbein, L. Ioffe, H. Knörrer, W. Kohn, U. Ledermann, K. LeHur, W. Metzner, M. Troyer, E. Trubowitz, F. C. Zhang, and M. Zhitomirsky for valuable discussions. C.H. acknowledges financial support from the Swiss National Fonds.

APPENDIX A: RG TECHNIQUE

In this appendix we derive and discuss the RG equation for the 1PI functions. The RG equation for the 1PI functions was first used by Wetterich[35] in scalar field theory. In the following, we give a largely simplified, self-contained derivation of this equation for general fermion systems, and discuss the consequences of symmetries, as well as truncation schemes. We first recall the definition and those properties of the 1PI functions that we need in the derivation. In the following, we shall not need all the details of the specific setup in our model; we shall only use that the fermion propagator $\mathbf{C}_s$ depends on a parameter s. In our application, s is the scale parameter, e.g., $s = \log \Lambda$, where Λ is the flowing energy scale.

1. Generating function of the 1PI vertices

In a general theory with fermionic fields, the fields $\psi(X)$ and $\overline{\psi}(X)$ are labeled by an index X which comprises space-time, spin, flavor, and possible other indices. We collect ψ and $\overline{\psi}$ into a single vector $\Psi = (\overline{\psi}, \psi)$. We also use the notation $(A,B) = \int dX\, A(X) B(X)$, where $\int dX$ stands for summation over the discrete indices and integrals over the continuous ones. In the Hubbard model, the standard functional integral representation (see, e.g., Ref. 20, Sec. 4.2) gives $X = (\tau, \mathbf{x}, \sigma, c)$, where $\mathbf{x}$ is the position, $\sigma = \pm$ the third component of the spin, $-\beta/2 \leqslant \tau < \beta/2$ the usual Euclidean time used to convert the grand canonical trace to a functional integral over the Grassmann fields Ψ, and the charge index $c = \pm$ distinguishes between the components ψ and $\overline{\psi}$ of Ψ.

The generating function for the connected Green functions is defined by

$$e^{-W(H)} = \int d\mu_C(\Psi) e^{-\mathcal{V}(\Psi) + (H,\Psi)}. \tag{A1}$$

Here the Gaussian integral is given by an invertible operator $\mathbf{Q}$ with integral kernel $\mathbf{Q}(X,X')$. Because of the Grassmann nature of the fields, $\mathbf{Q}$ is antisymmetric, i.e., $\mathbf{Q}(X',X) = -\mathbf{Q}(X,X')$. The covariance $\mathbf{C}$ is $\mathbf{C} = \mathbf{Q}^{-1}$, and $d\mu_{\mathbf{C}}(\Psi) = (\det \mathbf{Q})^{-1} e^{-1/2(\Psi, \mathbf{Q}\Psi)} D\overline{\psi}\, D\psi$, with (A,B) as defined above. A general $\mathbf{Q}$ gives rise to non-charge-invariant terms of type $\psi(X)\psi(X')$; charge invariance corresponds to a $\mathbf{Q}$ of the form

$$[\mathbf{Q}(\xi,\xi')]_{cc'} = \begin{pmatrix} 0 & Q(\xi,\xi') \\ -Q(\xi',\xi) & 0 \end{pmatrix}. \tag{A2}$$

In the Hubbard model [with $\xi = (\tau, \mathbf{x}, \sigma)$],

$$Q(\xi,\xi') = \delta_{\sigma\sigma'} \delta(\tau - \tau') [\delta_{\mathbf{x}\mathbf{x}'} (\partial_\tau + \mu) - T_{\mathbf{x}\mathbf{x}'}], \tag{A3}$$

where T denotes the hopping matrix. $\mathcal{V}$ is the interaction written in terms of the fields Ψ (for details, see, e.g., Ref. 20). The source term H is another Grassmann vector; if $H = \begin{pmatrix} -\eta \\ \overline{\eta} \end{pmatrix}$, then (H,Ψ) is the usual combination $(\overline{\eta}, \psi) + (\overline{\psi}, \eta)$.

The action in the functional integral has all symmetries of the Hubbard Hamiltonian. The action and the integration measure are also invariant under the transformation

$$\psi_\sigma(\tau,\mathbf{x}) \to i\overline{\psi}_\sigma(-\tau,\mathbf{x}), \quad \overline{\psi}_\sigma(\tau,\mathbf{x}) \to i\psi_\sigma(-\tau,\mathbf{x}). \tag{A4}$$

Observables transform accordingly (similarly as when taking adjoints).

If W has a nondegenerate quadratic part, the map $H \mapsto \Phi_{cl}(H)$, with

$$\Phi_{cl}(H)(X) = \frac{\delta}{\delta H(X)} W(H), \tag{A5}$$

can be inverted (this is the case in our fermionic models because the Grassmann variables are nilpotent and the covariance $\mathbf{C}$ is nondegenerate at positive temperature. In bosonic models, the map would not be invertible if symmetry breaking occurs. The Legendre transform is then defined by a variational equation; see, e.g., Ref. 36). Denote the inverse map by $\phi \mapsto h(\phi)$ (h is an odd element of the Grassmann algebra generated by ϕ), so that

$$\Phi_{cl}[h(\phi)] = \frac{\delta W}{\delta H}[h(\phi)] = \phi. \tag{A6}$$

Taking a derivative with respect to ϕ gives

$$\int dZ \frac{\delta h(\phi)(Z)}{\delta \phi(Y)} \left(\frac{\delta^2 W}{\delta H(Z)\delta H(X)} \right)[h(\phi)] = \delta(X,Y). \tag{A7}$$

The first Legendre transform of W is

$$\Gamma(\phi) = W[h(\phi)] - [h(\phi), \phi] \tag{A8}$$

(with the last term a bilinear form as above); it generates the 1PI correlation functions. We have $\delta\Gamma/\delta\phi = h(\phi)$, and thus by Eq. (A7) (as operators),

$$\left(\frac{\delta^2 \Gamma}{\delta \phi^2} \right)(\phi) = \left[\frac{\delta^2 W}{\delta H^2}[h(\phi)] \right]^{-1}. \tag{A9}$$

For free particles ($\mathcal{V}=0$), $W = \frac{1}{2}(H, \mathbf{C}H)$, so $\delta W/\delta H = \mathbf{C}H$; hence $h(\phi) = \mathbf{C}^{-1}\phi$ and $\Gamma(\phi) = \frac{1}{2}(\phi, \mathbf{Q}\phi)$. In first order, the four-fermion interaction term in Γ is just the original interaction $\mathcal{V}$.

2. RG differential equation for Γ

If W depends on a parameter s, then Γ and h also depend on s. By Eq. (A6),

$$\frac{d}{ds} W_s[h_s(\phi)] = \frac{\partial W_s}{\partial s}[h_s(\phi)] + [\dot{h}_s(\phi), \phi] \tag{A10}$$

(where the dot denotes the derivative with respect to s), so Eq. (A8) implies

$$\dot{\Gamma}_s(\phi) = \dot{W}_s[h_s(\phi)]. \tag{A11}$$

We now assume that the s dependence of W_s is given as follows. In Eq. (A1), $\mathcal{V}$ remains independent of s, but $\mathbf{C}$ is replaced by $\mathbf{C}_s = \mathbf{Q}_s^{-1}$, where $\mathbf{Q}_s$ now depends on s. Then the derivative $\partial/\partial s$ can act only on $d\mu_{\mathbf{C}_s}$, that is, on the normalization factor or on the exponent. In the former case, it just produces a constant term; in the latter case it brings down $(\Psi, \dot{\mathbf{Q}}_s \Psi)$ in the integral. Using

$$(\Psi, \dot{\mathbf{Q}}_s \Psi) e^{(H,\Psi)} = \left(\frac{\delta}{\delta H}, \dot{\mathbf{Q}}_s \frac{\delta}{\delta H} \right) e^{(H,\Psi)}, \tag{A12}$$

we can reexpress everything in terms of $W_s(H)$, and obtain

$$\dot{W}_s(H) = \frac{1}{2}\mathrm{Tr}(\mathbf{C}_s \dot{\mathbf{Q}}_s) + \frac{1}{2}\left(\frac{\delta W_s}{\delta H}, \dot{\mathbf{Q}}_s \frac{\delta W_s}{\delta H} \right) + \frac{1}{2}\left(\frac{\delta}{\delta H}, \dot{\mathbf{Q}}_s \frac{\delta}{\delta H} \right) W_s(H), \tag{A13}$$

with $\mathrm{Tr}(AB) = \int dX\, dY\, A(X,Y)B(Y,X)$. This is an equation similar to Polchinski's equation,[37] but with $\mathbf{Q}_s$ instead of $\mathbf{C}_s$ in the Laplacian because the Green functions generated by W are not amputated. By Eqs. (A11), (A6), and (A9), the differential equation for $\Gamma(s)$ is

$$\dot{\Gamma}(s|\phi) = \frac{1}{2}\mathrm{Tr}(\mathbf{C}_s \dot{\mathbf{Q}}_s) + \frac{1}{2}(\phi, \dot{\mathbf{Q}}_s \phi) + \frac{1}{2}\mathrm{Tr}\left[\dot{\mathbf{Q}}_s \left(\frac{\delta^2 \Gamma(s|\phi)}{\delta \phi^2} \right)^{-1} \right]. \tag{A14}$$

This is a nonpolynomial equation for Γ, but the inverse contains a second derivative, which produces a field-independent term coming from the quadratic term in Γ. Thus the equation makes sense in an expansion in the fields.

3. Expansion in the fields

In this section we derive the equation for the scale-dependent 1PI m-point functions $\gamma_m(s)$, by expanding $\Gamma(s|\phi)$ in the fields. Readers that only want to see the result can skip to Appendix A 4.

The 1PI m-point vertex functions $\gamma_m(s|X_1, \ldots, X_m)$ are the coefficients in an expansion of Γ as a power series in the fields,

$$\Gamma(s|\phi) = \sum_{m \geq 0} \gamma^{(m)}(s|\phi), \tag{A15}$$

with

$$\gamma^{(m)}(s|\phi) = \frac{1}{m!} \int d^m \underline{X}\, \gamma_m(s|\underline{X}) \phi^m(\underline{X}). \tag{A16}$$

Here we used the notations $\underline{X} = (X_1, \ldots, X_m)$ and $\phi^m(\underline{X}) = \phi(X_1) \cdots \phi(X_m)$. Because the Grassmann variables anticommute, we choose the function $\gamma_m(s|\underline{X})$ to be totally antisymmetric with respect to permutations of the X_i. This allows us to compare coefficients. $\gamma_m(s|\underline{X})$ are the 1PI vertex functions. Similarly, we have the expansion

$$\frac{\delta}{\delta \phi(X)} \frac{\delta}{\delta \phi(Y)} \Gamma(s|\phi) = \sum_{m \geq 0} \tilde{\gamma}^{(m)}(s|X, Y; \phi). \tag{A17}$$

By the antisymmetry of γ_m, two derivatives applied to $\gamma^{(m+2)}$ give a factor $(m+2)(m+1)$, which combines with the $1/(m+2)!$ to $1/m!$ [this is the reason for the convention of putting the prefactor $1/m!$ in Eq. (A16)]. Thus

$$\tilde{\gamma}^{(m)}(s|X,Y;\phi)=\frac{1}{m!}\int d^m\underline{X}'\,\gamma_{m+2}(s|X,Y,\underline{X}')\,\phi^m(\underline{X}'). \tag{A18}$$

In particular, $\tilde{\gamma}^{(0)}$ is independent of ϕ:

$$\tilde{\gamma}^{(0)}(s|X,Y;\phi)=\gamma_2(s|X,Y). \tag{A19}$$

Therefore,

$$\frac{\delta^2\Gamma(s|\phi)}{\delta\phi(X)\,\delta\phi(Y)}=\gamma_2(s|X,Y)+\tilde{\Gamma}(s|X,Y;\phi), \tag{A20}$$

with

$$\tilde{\Gamma}(s|X,Y;\phi)=\sum_{m\geqslant 2}\tilde{\gamma}^{(m)}(s|X,Y;\phi). \tag{A21}$$

It is natural to think of $\gamma_2(s|X,Y)$ and of $\tilde{\Gamma}(s|X,Y;\phi)$ as integral kernels of operators γ_2 and $\tilde{\Gamma}(s|\phi)$. By relation (A9), at $\phi=0$,

$$\mathbf{G}_s=\gamma_2(s)^{-1} \tag{A22}$$

is the full two-point function. As an equation between operators, we thus have

$$\frac{\delta^2\Gamma}{\delta\phi^2}(s|\phi)=\gamma_2[1+\mathbf{G}_s\tilde{\Gamma}(s|\phi)], \tag{A23}$$

so the differential equation for Γ now reads

$$\dot{\Gamma}(s|\phi)=\tfrac{1}{2}\,\mathrm{Tr}(\mathbf{C}_s\dot{\mathbf{Q}}_s)+\tfrac{1}{2}\,(\phi,\dot{\mathbf{Q}}_s\phi)+\tfrac{1}{2}\,\mathrm{Tr}\{\mathbf{G}_s\dot{\mathbf{Q}}_s[1+\mathbf{G}_s\tilde{\Gamma}(s|\phi)]^{-1}\} \tag{A24}$$

To perform the expansion in the fields, we first use the geometric series

$$\begin{aligned}\mathrm{Tr}\{\mathbf{G}_s\dot{\mathbf{Q}}_s[1+\mathbf{G}_s\tilde{\Gamma}(s|\phi)]^{-1}\}&=\mathrm{Tr}(\mathbf{G}_s\dot{\mathbf{Q}}_s)-\mathrm{Tr}[\mathbf{G}_s\dot{\mathbf{Q}}_s\mathbf{G}_s\tilde{\Gamma}(s|\phi)]\\&\quad+\sum_{p\geqslant 2}(-1)^p\,\mathrm{Tr}\{\mathbf{G}_s\dot{\mathbf{Q}}_s[\mathbf{G}_s\tilde{\Gamma}(s|\phi)]^p\}.\end{aligned} \tag{A25}$$

The first term is a constant, which corresponds to a vacuum energy, and is not interesting for our purposes because it drops out in all correlation functions. The term linear in $\tilde{\Gamma}$ generates contractions with single lines; its lowest order in ϕ is quadratic in ϕ, and therefore generates self-energy corrections. The graphical interpretation of the terms with $p\geqslant 2$ is also straightforward: The pth order term $[\mathbf{G}_s\tilde{\Gamma}(s,\phi)]^p\mathbf{G}_s$ is a linear tree with p vertices. Taking the trace with $\dot{\mathbf{Q}}_s$ forms a loop. Thus only 1PI graphs contribute to the graphical expansion for Γ.

We define the single-scale propagator as

$$\mathbf{S}_s=-\mathbf{G}_s\dot{\mathbf{Q}}_s\mathbf{G}_s\,. \tag{A26}$$

$\tilde{\gamma}^{(m)}$ defined in Eq. (A18) are homogeneous of degree m in ϕ; inserting Eq. (A15) on the left-hand side and Eq. (A21) on the right-hand side of Eq. (A24), we obtain a system of equations for $\gamma^{(m)}$. For $m\leqslant 6$ the equations are

$$\begin{aligned}\dot{\gamma}^{(2)}(s|\phi)&=\tfrac{1}{2}\,(\phi,\dot{\mathbf{Q}}_s\phi)+\tfrac{1}{2}\,\mathrm{Tr}[\mathbf{S}_s\tilde{\gamma}^{(2)}(s|\phi)]\\\dot{\gamma}^{(4)}(s|\phi)&=\tfrac{1}{2}\,\mathrm{Tr}[\mathbf{S}_s\tilde{\gamma}^{(4)}(s|\phi)]-\tfrac{1}{2}\,\mathrm{Tr}[\mathbf{S}_s\tilde{\gamma}^{(2)}(s|\phi)\mathbf{G}_s\tilde{\gamma}^{(2)}(s|\phi)]\\\dot{\gamma}^{(6)}(s|\phi)&=\tfrac{1}{2}\,\mathrm{Tr}[\mathbf{S}_s\tilde{\gamma}^{(6)}(s|\phi)]-\tfrac{1}{2}\,\mathrm{Tr}[\mathbf{S}_s(\tilde{\gamma}^{(4)}\mathbf{G}_s\tilde{\gamma}^{(2)}+\tilde{\gamma}^{(2)}\mathbf{G}_s\tilde{\gamma}^{(4)})]+\tfrac{1}{2}\,\mathrm{Tr}[\mathbf{S}_s\tilde{\gamma}^{(2)}\mathbf{G}_s\tilde{\gamma}^{(2)}\mathbf{G}_s\tilde{\gamma}^{(2)}].\end{aligned} \tag{A27}$$

4. RGDE for two- and four-point vertexes

Denote $\underline{Y}=(Y_1,\ldots,Y_4)$,

$$\mathbf{L}(\underline{Y})=\mathbf{S}_s(Y_1,Y_2)\mathbf{G}_s(Y_3,Y_4)++\mathbf{S}_s(Y_3,Y_4)\mathbf{G}_s(Y_1,Y_2), \tag{A28}$$

with $\mathbf{S}_s$ as in Eq. (A26) and $\mathbf{G}_s$ as in Eq. (A22) and

$$\begin{aligned}\mathbf{B}_s(\underline{X},\underline{Y})&=\gamma_4(s|X_1,X_2,Y_2,Y_3)\,\gamma_4(s|Y_4,Y_1,X_3,X_4)\\&\quad-\gamma_4(s|X_1,X_3,Y_2,Y_3)\,\gamma_4(s|Y_4,Y_1,X_2,X_4)\\&\quad+\gamma_4(s|X_1,X_4,Y_2,Y_3)\,\gamma_4(s|Y_4,Y_1,X_2,X_3).\end{aligned} \tag{A29}$$

The differential equation for the 1PI four-point function γ_4 is

$$\begin{aligned}\dot{\gamma}_4(s|\underline{X})&=\tfrac{1}{2}\int dY_1\,dY_2\,\gamma_6(s|\underline{X},Y_1,Y_2)\mathbf{S}_s(Y_2,Y_1)\\&\quad-\tfrac{1}{2}\int d^4\underline{Y}\,\mathbf{L}(\underline{Y})\mathbf{B}_s(\underline{X},\underline{Y}).\end{aligned} \tag{A30}$$

From Eqs. (A18) and (A19), the equation for the 1PI two-point function γ_2 becomes

$$\begin{aligned}\dot{\gamma}_2(s|X_1,X_2)&=\dot{\mathbf{Q}}_s(X_1,X_2)+\tfrac{1}{2}\int dX_3\,dX_4\,\mathbf{S}_s(X_4,X_3)\\&\quad\times\gamma_4(s|X_1,X_2,X_3,X_4).\end{aligned} \tag{A31}$$

Equations (A30) and (A31) are the first two equations in the infinite system of RG equations (labeled by m). Note that they do not form a closed system because γ_6 enters into Eq. (A30). This behavior continues to all m: the right-hand side of the equation for $\dot{\gamma}_m$ contains γ_{m+2}.

A way to close the system of equations for the 1PI four-point function γ_4 and the self-energy is to drop the 1PI six-point vertex from Eq. (A30). This truncation is equivalent to setting all 1PI functions with $m\geqslant 6$ external legs to zero, so that the connected (non-1PI) m-point functions with $m\geqslant 6$ are given by tree graphs made of four-legged vertices, and the approximation to the full propagator provided by the solution of the differential equations. The four- and two-point differential equations are given in terms of one-loop diagrams.

Note, however, that even an untruncated system of differential equations only contains one-loop terms in every equa-

tion. This is so because in the differential formulation, only one differentiated propagator appears in the equation (and there are no tree terms in an equation for 1PI functions). Of course, this does not imply that only one-loop graphs appear in the solution; the full RG produces, after all, the full Green functions. The perturbation expansion is obtained by integrating the differential equation from 0 to s and then iterating the thus-obtained integral equation until only bare vertices appear. Upon iteration, graphs with an arbitrary number of loops are generated; if one uses the untruncated equations, all graphs are generated. The truncated equations amount to a summation of part of the diagrams, but these diagrams also contain two-loop graphs, in particular two-loop graphs corresponding to the self-energy. The RG strategy does not necessarily aim at taking into account as many graphs as possible but to single out the important ones by their scaling behavior.

The initial condition for γ_4 is the bare interaction. To renormalize the Fermi surface correctly, one also needs to take into account a Fermi-surface counterterm (see Refs. 38 and 39). In the bulk of this paper, we neglect the self-energy correction. Then $\mathbf{G}_s = \mathbf{C}_s$ and $\mathbf{S}_s = \dot{\mathbf{C}}_s$, and no Fermi-surface counterterm is needed. However, in the general discussion given in this appendix, we keep the self-energy to give the more general formulas. Equations for the full Fermi surface flow that do not require counterterms but use a dynamically changing propagator, appear in Ref. 40.

5. Consequences of symmetries

The derivation of Eqs. (A30) and (A31) did not require any symmetries, so these equations are also valid when symmetries are broken. In our systems, this means that they also hold in the presence of a superconducting gap or magnetic ordering or translational symmetry breaking. In two dimensions, continuous symmetry breaking is impossible at any positive temperature by the Mermin-Wagner theorem. A noninvariance of the effective action leads immediately to long-range order, and hence mean-field-type results. In order to compare competing instabilities, we therefore first assume that all continuous symmetries of the action remain unbroken. This leads to further simplifications in the differential equations, which we now successively discuss.

a. Charge invariance

Recalling that $X=(\xi,c)$ where ξ consists of space, time, and spin indices, and where $c=\pm$ is the charge index, charge invariance implies that $\mathbf{S}_s[(\xi,c),(\xi',c')]$ and $\mathbf{G}_s[(\xi,c),(\xi',c')]$ are nonzero only if $c\neq c'$, and that $\gamma_4(s|X_1,\ldots,X_4)\neq 0$ only if two of the charge indices are $+$ and two are $-$. Because γ_4 is antisymmetric in all arguments, it is then determined by $f(s|\xi_1,\ldots,\xi_4) = \gamma_4[s|(\xi_1,+),(\xi_2,+),(\xi_3,-),(\xi_4,-)]$. Also, f inherits the antisymmetry under exchange of ξ_1 and ξ_2 and that under exchange of ξ_3 and ξ_4.

Equation (A30) gives the following equation for f:

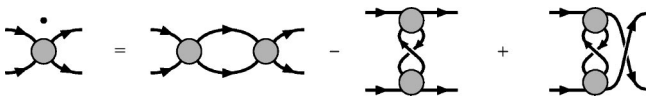

FIG. 14. The RGDE for f.

$$\dot{f}(s|\xi_1,\xi_2,\xi_3,\xi_4) = \Phi_{\rm pp}(s|\xi_1,\xi_2,\xi_3,\xi_4) + \Phi_{\rm ph}(s|\xi_1,\xi_2,\xi_3,\xi_4) - \Phi_{\rm ph}(s|\xi_1,\xi_2,\xi_4,\xi_3), \quad \text{(A32)}$$

with

$$\Phi_{\rm pp}(s|\xi_1,\ldots,\xi_4) = \tfrac{1}{2}\int d\eta_1,\ldots,d\eta_4\, L(\eta_2,\eta_1,\eta_3,\eta_4) \times f(s|\xi_1,\xi_2,\eta_2,\eta_3) f(s|\eta_4,\eta_1,\xi_3,\xi_4) \quad \text{(A33)}$$

and

$$\Phi_{\rm ph}(s|\xi_1,\ldots,\xi_4) = -\int d\eta_1,\ldots,d\eta_4\, L(\eta_1,\eta_2,\eta_3,\eta_4) \times f(s|\eta_4,\xi_2,\xi_3,\eta_1) f(s|\xi_1,\eta_2,\xi_4), \quad \text{(A34)}$$

and where

$$L(\eta_1,\ldots,\eta_4) = S_s(\eta_1,\eta_2)G_s(\eta_3,\eta_4) + G_s(\eta_1,\eta_2)S_s(\eta_3,\eta_4). \quad \text{(A35)}$$

There is no $\frac{1}{2}$ in $\Phi_{\rm ph}$ because there are twice as many terms in the sum over intermediate charge indices c_i in the $\Phi_{\rm ph}$ as in $\Phi_{\rm pp}$. The function $\Phi_{\rm pp}$ is antisymmetric under exchange of (ξ_1,ξ_2) and (ξ_3,ξ_4), because f has these properties. The function $\Phi_{\rm ph}$ is not, but the difference appearing in Eq. (A32) is antisymmetric.

Equation (A32) has the graphical representation shown in Fig. 14. The internal lines in these graphs correspond to ''full'' propagators G_s, and to single scale propagators S_s, respectively. The inverse of G_s is $g_2(s|\xi_1,\xi_2) = \gamma_2[s|(\xi_1,+),(\xi_2,-)]$, and satisfies

$$\dot{g}_2(s|\xi_1,\xi_2) = \dot{Q}_s(\xi_1,\xi_2) - \int d\xi_1\, d\xi_2\, S_s(\xi_4,\xi_3) f(s|\xi_1,\xi_3,\xi_4,\xi_2). \quad \text{(A36)}$$

b. Spin rotation invariance

We now derive the consequences of SU(2) invariance.

The initial interaction of important many-fermion models has the SU(2) spin invariance. For instance, the initial Hubbard interaction, and interactions of the form $S_x S_y$, where $S_x = \overline{\psi}(x)(\sigma/2)\psi(x)$ is the spin at x, have this property.

Spin rotation invariance restricts the form of f as follows. If we define a spin tensor

$$F(s|x_1,\ldots,x_4)_{\sigma_1\ldots\sigma_4}=f[s|(x_1,\sigma_1),\ldots,(x_4,\sigma_4)]; \tag{A37}$$

then

$$F(s|x_1,\ldots,x_4)=-\varphi(s|x_1,x_2,x_3,x_4)D + \tilde{\varphi}(s|x_1,x_2,x_3,x_4)E, \tag{A38}$$

where $D_{\sigma_1,\ldots,\sigma_4}=\delta_{\sigma_1\sigma_3}\delta_{\sigma_2\sigma_4}$ and $E_{\sigma_1,\ldots,\sigma_4}=\delta_{\sigma_1\sigma_4}\delta_{\sigma_2\sigma_3}$.

The equation $E_{\sigma_2\sigma_1\sigma_3\sigma_4}=D_{\sigma_1\sigma_2\sigma_3\sigma_4}$ and the antisymmetry of f under $(x_1,\sigma_1)\leftrightarrow(x_2,\sigma_2)$ imply that

$$\tilde{\varphi}(s|x_1,x_2,x_3,x_4)=\varphi(s|x_2,x_1,x_3,x_4) =\varphi(s|x_1,x_2,x_4,x_3). \tag{A39}$$

Exchanging twice, we have [similarly to Eq. (A39)]

$$\varphi(s|x_2,x_1,x_4,x_3)=\varphi(s|x_1,x_2,x_3,x_4). \tag{A40}$$

However there is no symmetry of φ under exchange of only one pair of coordinates.

The Fierz identity

$$\sum_{i=1}^{3}(\sigma^i)_{\mu\nu}(\sigma^i)_{\alpha\beta}=2\delta_{\alpha\nu}\delta_{\beta\mu}-\delta_{\mu\nu}\delta_{\alpha\beta} \tag{A41}$$

implies that interactions of the form S_xS_y can be written in the form of Eq. (A38). Using Eq. (A41), one can also reconstruct the four-fermion interaction in the form $\tilde{S}\tilde{S}+\tilde{\rho}\tilde{\rho}$, where $\tilde{S}$ and $\tilde{\rho}$ transform like spin densities and charge densities as concerns the spin dependence. For a general φ, $\tilde{S}$ and $\tilde{\rho}$ will involve fields at different space-time points.

The renormalization group differential equation (RGDE) for φ takes the form

$$\dot{\varphi}(s)=\mathcal{T}_{\rm pp}(s)+\mathcal{T}^d_{\rm ph}(s)+\mathcal{T}^{\rm tr}_{\rm ph}(s), \tag{A42}$$

where, using $\underline{x}=(x_1,x_2,x_3,x_4)$,

$$\mathcal{T}_{\rm pp}(s|\underline{x})=-\int dy_1,\ldots,dy_4\,L(y_1,y_3,y_2,y_4) \times\varphi(s|x_1,x_2,y_1,y_2)\varphi(s|y_3,y_4,x_3,x_4), \tag{A43}$$

$$\mathcal{T}^d_{\rm ph}(s|x)=-\int dy_1,\ldots,dy_4\,L(y_1,y_2,y_4,y_3) \times[-2\varphi(s|x_2,y_2,x_4,y_4)\varphi(s|x_1,y_3,x_3,y_1) +\varphi(s|x_2,y_2,x_4,y_4)\varphi(s|x_1,y_3,y_1,x_3) \times\varphi(s|x_2,y_2,y_4,x_4)\varphi(s|x_1,y_3,x_3,y_1)], \tag{A44}$$

$$\mathcal{T}^{\rm cr}_{\rm ph}(s|\underline{x})=-\int dy_1,\ldots,dy_4(y_1,y_3,y_2,y_4) \times\varphi(s|x_2,y_3,y_2,x_3)\varphi(s|x_1,y_4,y_1,x_4), \tag{A45}$$

and

$$L(y_1,y_2,y_3,y_4)=S(y_1,y_2)G(y_3,y_4)+G(y_1,y_2)S(y_3,y_4).$$

Similarly, the equation for the full inverse two-point function is

$$\dot{\gamma}_2(s|x_1,x_2)=\dot{q}_s(x_1,x_2)-\dot{\Sigma}_s(x_1,x_2) \tag{A46}$$

with a scale-dependent self-energy Σ_s that satisfies

$$\dot{\Sigma}_s(x_1,x_2)=\int dx_3\,dx_4\,S_s(x_4,x_3)[-2\varphi(s|x_1,x_3,x_2,x_4) +\varphi(s|x_1,x_3,x_4,x_2)]. \tag{A47}$$

The initial condition for Σ_s depends on how the Fermi surface is renormalized.

The graphical interpretation of the equations for φ is given in the bulk of the paper. The symmetry [Eq. (A4)] implies that

$$\varphi(s|x_1,x_2,x_3,x_4)=\overline{\varphi(s|Rx_4,Rx_3,Rx_2,Rx_1)}, \tag{A48}$$

where $R(\tau,\mathbf{x})=(-\tau,\mathbf{x})$. Similarly, the self-energy satisfies

$$\Sigma_s(x_1,x_2)=\overline{\Sigma_s(Rx_1,Rx_2)}. \tag{A49}$$

c. Translation invariance

If translation invariance is unbroken, we can take the Fourier transform. In contrast to charge and spin invariance, translation invariance is only discrete in our lattice model, and thus may also be broken at positive temperature in two dimensions. Thus specializing to unbroken translation invariance is a further assumption. It can be relaxed if one assumes that invariance under a sufficiently large subgroup, e.g., that of translations of a sublattice, still holds. The corresponding Fourier transform is then defined on a smaller momentum space.

We take the convention that momenta corresponding to $\overline{\psi}$ are counted outgoing and those corresponding to ψ are counted as incoming. Then translation invariance implies that $\hat{\varphi}(s|p_1,p_2,p_3,p_4)=\delta(p_1+p_2-p_3-p_4)V_s(p_1,p_2,p_3)$, and the equation for V_s reads $\dot{V}_s=\hat{\mathcal{T}}_{\rm pp}+\hat{\mathcal{T}}^d_{\rm ph}+\hat{\mathcal{T}}^{\rm cr}_{\rm ph}$, with the particle-particle term

$$\dot{\mathcal{T}}_{\rm pp}(p_1,p_2,p_3)=-\int dk\,\mathcal{L}_-(p_1+p_2,k)V_s(p_1,p_2,k) \times V_s(k,p_1+p_2-k,p_3), \tag{A50}$$

the direct particle-hole term

$$\hat{\mathcal{T}}^d_{\rm ph}(p_1,p_2,p_3) =-\int dk\,\mathcal{L}_+(p_1-p_3,k) \times[-2V_s(p_1,k,p_3)V_s(k+p_1-p_3,p_2,k) +V_s(p_1,k,k+p_1-p_3)V_s(k+p_1-p_3,p_2,k) +V_s(p_1,k,p_3)V_s(p_2,k+p_1-p_3,k)], \tag{A51}$$

and the crossed particle-hole term

$$\hat{\mathcal{T}}^{\mathrm{cr}}_{\mathrm{ph}}(p_1,p_2,p_3) = -\int dk\, \mathcal{L}_+(p_2-p_3,k) \times V_s(p_1,k+p_2-p_3,k) V_s(k,p_2,p_3). \tag{A52}$$

Here

$$\mathcal{L}_\pm(q,k) = \hat{S}(k)\hat{G}(q\pm k) + \hat{S}(q\pm k)\hat{G}(k). \tag{A53}$$

The symmetry [Eq. (A48)] implies that

$$V_s(p_1,p_2,p_3) = \overline{V_s(R(p_1+p_2-p_3),Rp_3,Rp_2)}, \tag{A54}$$

with $R(\omega,\mathbf{p}) = (-\omega,\mathbf{p})$.

6. Flow of the susceptibilities

As discussed in the text, the susceptibilities are obtained by coupling external boson fields to the bilinears in the fermions that represent charge, spin, Cooper pair, and other local densities, and by calculating the corresponding RG flow for these functions. Since the calculations are a straightforward adaptation of the ones presented above, we only state the main points. If the external field is called a, the expansion of Γ_s now reads $\Gamma_s(a,\phi) = \Sigma_{m,n\geq 0}\gamma^{(m,n)}(s|a,\phi)$, with $\gamma^{(m,n)}(s|a,\phi) = (1/m!n!)\int d^m\underline{X}\, d^n\underline{Y}\, \gamma_{mn}(s,\underline{X},\underline{Y}) a^m(\underline{X})\phi^n(\underline{Y})$. The RGDE is now derived in the same way as above. Because the a fields are external fields only, the equations for the a-independent parts γ_{0n} remain unchanged, so that $\gamma_{0n} = \gamma_n$ for all n, with γ_n given as above. Thus the flow for the susceptibilities is driven by the flow for the coupling functions; it takes the form of a linear integro-differential equation.

Since one a field couples to a fermionic bilinear, the truncation consistent with dropping the 1PI six-point function is to leave out all m and n with $2m+n \geq 6$. This gives the equations

$$\dot{\gamma}_{12}(s|X;Y_1,Y_2) = \tfrac{1}{2}\int d^4\underline{Z}\, \mathbf{L}(Z_1,\ldots,Z_4)\, \gamma_{12}(s|X,Z_2,Z_3) \times \gamma_{04}(s|Z_4,Z_1;Y_1,Y_2) \tag{A55}$$

and

$$\dot{\gamma}_{20}(s|X_1,X_2) = \tfrac{1}{2}\int d^4\underline{Z}\, \mathbf{L}(Z_1,\ldots,Z_4) \times \gamma_{12}(s|X_1,Z_2,Z_3)\, \gamma_{12}(s|X_2;Z_4,Z_1), \tag{A56}$$

with $\mathbf{L}$ given by Eq. (A28). The initial condition on γ_{12} at $s=0$ determines which susceptibility is considered; in particular, it determines the symmetry of the superconducting order parameter in the case of the coupling to Cooper pairs.

In the presence of charge invariance, we obtain separate equations for the particle-particle and particle-hole vertices, defined as

$$\gamma^{\mathrm{pp},\epsilon}_{12}[s|x;(y_1,\sigma_1),(y_2,\sigma_2)] = \gamma_{12}[s|x;(y_1,\sigma_1,\epsilon),(y_2,\sigma_2,\epsilon)] \tag{A57}$$

and

$$\gamma^{\mathrm{ph},\epsilon}_{12}[s|x;(y_1,\sigma_1),(y_2,\sigma_2)] = \gamma_{12}[s|x;(y_1,\sigma_1,\epsilon),(y_2,\sigma_2,-\epsilon)]. \tag{A58}$$

By fermionic antisymmetry, $\gamma^{\mathrm{pp},-}_{12}[s|x;(y_1,\sigma_1),(y_2,\sigma_2)] = -\gamma^{\mathrm{pp},+}_{12}[s|x;(y_2,\sigma_2),(y_1,\sigma_1)]$ and similarly for $\gamma^{\mathrm{ph},\pm}_{12}$, so it suffices to consider one of the $\pm$ quantities. We now also assume spin rotation invariance; then the normal charge ($\sim\delta_{\sigma_1\sigma_2}$) and spin $\sim(\tau_3)_{\sigma_1\sigma_2}$ susceptibility (τ_3 the Pauli matrix) do not couple in the flow. The resulting equations are

$$\dot{\gamma}^{\mathrm{pp},-}_{12}[s|x;(y_1,\sigma_1),(y_2,\sigma_2)] = \int du_1,\ldots,du_4\, L(u_1,u_2,u_3,u_4) \times \gamma^{\mathrm{pp},-}_{12}[s|x;(u_1,\sigma_1),(u_3,\sigma_2)] \times \varphi(s|u_2,u_4,y_1,y_2) \tag{A59}$$

for the Cooper pair vertex

$$\dot{\gamma}_{12,\mathrm{charge}}(s|x;y_1,y_2) = \int du_1,\ldots,du_4\, \mathrm{Re}\, L(u_1,u_2,u_3,u_4) \times \gamma_{12,\mathrm{charge}}(s|x;u_4,u_1)[2\varphi(s|y_1,u_2,y_2,u_3) - \varphi(s|y_1,u_2,u_3,y_2)] \tag{A60}$$

for the charge vertex, and

$$\dot{\gamma}_{12,\mathrm{spin}}(s|x;y_1,y_2) = \int du_1,\ldots,du_4\, \mathrm{Re}\, L(u_1,u_2,u_3,u_4) \times \gamma_{12,\mathrm{spin}}(s|x;u_4,u_1)\varphi(s|y_1,u_2,u_3,y_2) \tag{A61}$$

for the spin vertex. The corresponding susceptibilities are then obtained from Eq. (A56).

APPENDIX B: CALCULATION OF THE UNIFORM SUSCEPTIBILITIES

The uniform ($\mathbf{q}\to 0$) susceptibilities describing the response to external charges and magnetic fields cannot be calculated successively by lowering the IR cutoff, as they only involve degrees of freedom very close to the FS (the width of this region is given by the temperature). Therefore, we determine these responses for the effective theory below the cutoff Λ with the interactions at this scale as the effective interactions renormalizing the coupling to the external fields via vertex corrections. More precisely, we calculate the effective couplings $h_i(\mathbf{k})$ ($i=c$ for charge and $i=s$ for spin) of quasiparticles on the FS, occurring in the Hamiltonian as

$$\int \frac{d\mathbf{k}}{(2\pi)^2} h_{c/s}(\mathbf{k})(c^\dagger_{\vec{k},\uparrow}c_{\vec{k},\uparrow} \pm c^\dagger_{\vec{k},\downarrow}c_{\vec{k},\downarrow}).$$

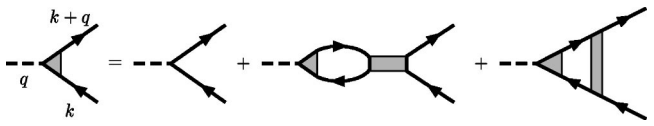

FIG. 15. Diagrammatic expression for the renormalization of the couplings $h_{c/s}(\mathbf{k})$ to external charge or magnetic fields. For uniform external fields, we take $\mathbf{q}\rightarrow 0$.

Denoting the bare coupling as $h^0_{c/s}$, we can express the effective coupling as

$$h_i(\mathbf{k}) = h_i^0(\mathbf{k}) + \int \frac{d\mathbf{k}'}{(2\pi)^2} h_i(\mathbf{k})\Phi(\mathbf{k}')V_i(\mathbf{k},\mathbf{k}'), \quad i=c,s, \tag{B1}$$

where $V_c(\mathbf{k},\mathbf{k}') = [-V_\Lambda(\mathbf{k},\mathbf{k}',\mathbf{k}') + 2V_\Lambda(\mathbf{k},\mathbf{k}',\mathbf{k})]$ for the charge and $V_s(\mathbf{k},\mathbf{k}') = -V_\Lambda(\mathbf{k},\mathbf{k}',\mathbf{k}')$ for the spin coupling. Diagrammatically this equation is shown in Fig. 15. The kernel $\Phi(\mathbf{k})$ is $\omega=0$; then $\mathbf{q}\rightarrow 0$ is the limit of the Matsubara sum of the product of two propagators, and is given by the derivative of the Fermi function:

$$\Phi(\mathbf{k}) = \lim_{\vec{q}\rightarrow 0} \frac{n_F[\epsilon(\mathbf{k}+\mathbf{q})] - n_F[\epsilon(\mathbf{k})]}{\epsilon[(k+\mathbf{q}) - \epsilon(\mathbf{k})]} = \left.\frac{dn_F}{dE}\right|_{E=\epsilon(\mathbf{k})}. \tag{B2}$$

The uniform susceptibilities are then given as

$$\kappa = -\int \frac{d^2k}{(2\pi)^2} h_c^0(\mathbf{k})\Phi(\mathbf{k})h_c(\mathbf{k}), \tag{B3}$$

$$\chi_s(0) = -\int \frac{d^2k}{(2\pi)^2} h_s^0(\mathbf{k})\Phi(\mathbf{k})h_s(\mathbf{k}). \tag{B4}$$

In the absence of an instability the coupling functions for zero momentum transfer $V_\Lambda(\mathbf{k},\mathbf{k}',\mathbf{k}) - \frac{1}{2}V_\Lambda(\mathbf{k},\mathbf{k}',\mathbf{k}')$ and $-\frac{1}{2}V_\Lambda(\mathbf{k},\mathbf{k}',\mathbf{k}')$ would converge to the Landau interaction functions $f_s(\mathbf{k},\mathbf{k}')$ and $f_a(\mathbf{k},\mathbf{k}')$, respectively, and the expressions for the susceptibilities obtained with the above scheme reduce to the results from Fermi-liquid theory.

APPENDIX C: ONE-LOOP SELF-ENERGY AND FERMI-SURFACE SHIFT

Here is a short overview of the results for the RG flow of a Fermi surface with a fixed particle number. In order to obtain the FS flow we calculate in every RG step the change of the one-loop self-energy given by the contributions in Fig. 4. Due to the approximations made for the couplings, this self-energy is constant over a single patch, and only yields a patch-dependent shift of the Fermi surface. In order to keep the particle number fixed, we adjust the chemical potential after each step. Quite generally we find that the FS parts

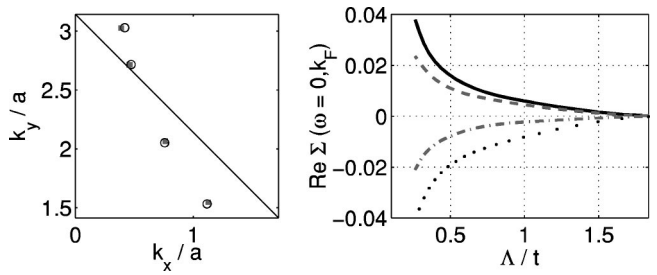

FIG. 16. Left: initial (open circles) and final (squares) FS for $t'=0.3t$ and $\langle n\rangle \approx 0.88$ per site. Right: flow of the self-energy on the FS (solid line: point closest to the saddle points; dotted line: point closest to BZ diagonal). The flow was stopped when the largest coupling reached the bandwidth $8t$.

which have the strongest repulsive scatterings with momentum transfer close to (π,π) develop positive self-energies, and are therefore shifted inward during the RG flow. The reason for this becomes clear if one considers a model interaction which is sharply peaked and repulsive at $\mathbf{Q}=(\pi,\pi)$. For the self-energy $\Sigma(\mathbf{k})$ of a particle with wave vector $\mathbf{k}$ on the FS, one primarily has to examine the Hartree term (the first term in Fig. 4), which is the main contribution for the typical divergence of the couplings. This diagram contains a propagator with a differentiated cutoff function, and gives a positive contribution if the state $\mathbf{k}+\mathbf{Q}$ is occupied, and a zero contribution otherwise. After subtraction of the FS average of $\Sigma(\mathbf{k}_F)$ (or more precisely a constant which keeps the particle number fixed), this yields a positive self-energy $\Sigma(\mathbf{k})>0$ for particles outside the US (because then in general the state $\mathbf{k}+\vec{Q}$ is occupied for a FS with the densities and t' values we are interested in) and a negative shift $\Sigma(\mathbf{k})<0$ for states inside the US. In our case the interaction only has a broad peak around (π,π); therefore, in general, FS points inside the BZ can also be pushed inward provided they are more affected by this repulsion than the average FS (this happens in the overdoped $\mu=-1.3t$ case). The flow of the the self-energies with fixed FS close to the instability is shown in Fig. 16(b) for different positions on the FS: for the FS points near the saddle points $\Sigma_\Lambda(\mathbf{k})$ flows to positive values, while for $\mathbf{k}_F$ in the BZ diagonal it becomes negative. The resulting movement of the FS points if we include $\Sigma_\Lambda(\mathbf{k})$ in the dispersion, i.e., allow the FS to move, can be seen in Fig. 16(a). It reveals the tendency of the FS to become flat, thus remaining in the vicinity of the umklapp surface.[41] In both cases the density is kept fixed at $\langle n\rangle \approx 0.88$ per site. Our RG results are in qualitative agreement with calculations using a model interaction due to AF spin fluctuations[42] and the FLEX approximation.[43]

*Present address.

[1] P. W. Anderson, *The Theory of Superconductivity in the High-T_c Cuprates* (Princeton University Press, Princeton, 1997).

[2] For a review, see T. Timusk and B. Statt, Rep. Prog. Phys. **62**, 61 (1999).

[3] E. Dagotto and T. M. Rice, Science **271**, 618 (1996).

[4] L. Balents and M. P. A. Fisher, Phys. Rev. B **53**, 12 133 (1996); H. Lin, L. Balents, and M. P. A. Fisher, *ibid.* **58**, 1794 (1998).

[5] M. P. A. Fisher, cond-mat/9806164 (unpublished), and references therein.

[6] T. M. Rice, S. Haas, M. Sigrist, and F. C. Zhang, Phys. Rev. B **56**, 14 655 (1997).

[7] I. Dzyaloshinskii, Zh. Eksp. Teor. Fiz. **93**, 1487 (1987) [Sov. Phys. JETP **66**, 848 (1987)]; I. Dzyaloshinskii, J. Phys. I **6**, 119

(1996).
[8] H. J. Schulz, Europhys. Lett. **4**, 609 (1987).
[9] P. Lederer, G. Montambaux, and D. Poilblanc, J. Phys. **48**, 1613 (1987).
[10] N. Furukawa, T. M. Rice, and M. Salmhofer, Phys. Rev. Lett. **81**, 3195 (1998).
[11] D. Zanchi and H. J. Schulz, Europhys. Lett. **44**, 235 (1997); Phys. Rev. B **61**, 13 609 (2000).
[12] C. J. Halboth and W. Metzner, Phys. Rev. B **61**, 7364 (2000).
[13] P. A. Lee, Physica C **317-318**, 194 (1999) [cond-mat/9812226 (unpublished)] and references therein.
[14] S. C. Zhang, Science **275**, 1089 (1997).
[15] M. Vojta and S. Sachdev, Phys. Rev. Lett. **83**, 3916 (1999).
[16] J. V. Alvarez, J. Gonzalez, F. Guinea, and M. A. H. Vozmediano, J. Phys. Soc. Jpn. **67**, 1868 (1998).
[17] J. Gonzalez, F. Guinea, and M. A. H. Vozmediano, Europhys. Lett. **34**, 711 (1996); Nucl. Phys. B **485**, 694 (1997).
[18] A. T. Zheleznyak, V. M. Yakovenko, and I. E. Dzyaloshinskii, Phys. Rev. B **55**, 3200 (1997).
[19] F. Vistulo de Abreu and B. Doucot, Europhys. Lett. **38**, 533 (1997).
[20] M. Salmhofer, *Renormalization*, Springer Texts and Monographs in Physics (Springer, Heidelberg, 1998).
[21] Below an energy scale determined by t'/t and μ, these terms become small compared to $\dot{d}_0$, which then dominates the flow. However if the initial coupling is not very weak, the coupling constants already diverge above that scale.
[22] M. Salmhofer and C. Honerkamp, Prog. Theor. Phys. (to be published).
[23] W. Kohn and J. M. Luttinger, Phys. Rev. Lett. **15**, 524 (1965).
[24] J. Feldman, H. Knörrer, R. Sinclair, and E. Trubowitz, Helv. Phys. Acta **70**, 154 (1997).
[25] W. Metzner, C. Castellani, and C. Di Castro, Adv. Phys. **47**, 317 (1998).
[26] N. Dupuis, Eur. Phys. J. B **3**, 315 (1998).
[27] As compared to an expansion in basis functions, this has the advantage that one can easily understand the dominant processes in momentum space.
[28] We have also calculated the flow including a radial dependence of V_Λ, by keeping three radial points in each patch [inside, on, and outside of the FS, i.e., $(32\times 3)^3$ coupling constants]. The main conclusions are the same as those without radial dependence.
[29] C. Bourbonnais, in *Strongly Interacting Fermions and High T_c Superconductivity, Les Houches 1991*, edited by B. Doucot and J. Zinn-Justin (North-Holland, Amsterdam, 1991).
[30] C. Honerkamp, Ph.D. thesis, ETH Zürich, 2000.
[31] V. B. Geshkenbein, L. B. Ioffe, and A. I. Larkin, Phys. Rev. B **55**, 3173 (1997).
[32] U. Ledermann, K. Le Hur, and T. M. Rice, cond-mat/0002445 (unpublished).
[33] M. R. Norman *et al.*, Nature (London) **392**, 157 (1998).
[34] L. B. Ioffe and A. J. Millis, Phys. Rev. B **58**, 11 631 (1998); V. B. Geshkenbein, L. B. Ioffe, and A. J. Millis, Phys. Rev. Lett. **80**, 5778 (1998).
[35] C. Wetterich, Z. Phys. C **57**, 451 (1993).
[36] B. Simon, *The Statistical Mechanics of Lattice Gases* (Princeton University Press, Princeton, 1993), Vol. 1.
[37] J. Polchinski, Nucl. Phys. B **231**, 269 (1984).
[38] M. Salmhofer, Rev. Math. Phys. **10**, 553 (1998).
[39] J. Feldman, M. Salmhofer, and E. Trubowitz, J. Stat. Phys. **84**, 1209 (1996); Commun. Pure Appl. Math. **51**, 1133 (1998); **52**, 273 (1999).
[40] M. Salmhofer (unpublished).
[41] In the $t'=0$ case close to half-filling, the states in the BZ diagonal are slightly more affected by the strong (π,π) repulsion than the states at the saddle points. Therefore, the FS expands toward the saddle points, although the trend is weaker than for $t'=0.3t$.
[42] Y. Yanase and K. Yamada, J. Phys. Soc. Jpn. **68**, 548 (1999).
[43] K. Morita and K. Miyake, Physica B **281**, 812 (2000).